Mesoscale modeling of Central American smoke transport to the United States: 1. "Top-down" assessment of emission strength and diurnal variation impacts

Jun Wang,[1,2] Sundar A. Christopher,[1] U. S. Nair,[1] Jeffrey S. Reid,[3] Elaine M. Prins,[4] James Szykman,[5,6] and Jenny L. Hand[7]

Received 27 June 2005; revised 29 August 2005; accepted 26 September 2005; published 9 March 2006.

[1] As is typical in the Northern Hemisphere spring, during 20 April to 21 May 2003, significant biomass burning smoke from Central America was transported to the southeastern United States (SEUS). A coupled aerosol, radiation, and meteorology model that is built upon the heritage of the Regional Atmospheric Modeling System (RAMS), having newly developed capabilities of Assimilation and Radiation Online Modeling of Aerosols (AROMA) algorithm, was used to simulate the smoke transport and quantify the smoke radiative impacts on surface energetics, boundary layer, and other atmospheric processes. This paper, the first of a two-part series, describes the model and examines the ability of RAMS-AROMA to simulate the smoke transport. Because biomass-burning fire activities have distinct diurnal variations, the FLAMBE hourly smoke emission inventory that is derived from the geostationary satellite (GOES) fire products was assimilated into the model. In the "top-down" analysis, ground-based observations were used to evaluate the model performance, and the comparisons with model-simulated results were used to estimate emission uncertainties. Qualitatively, a 30-day simulation of smoke spatial distribution as well as the timing and location of the smoke fronts are consistent with those identified from the $PM_{2.5}$ observation network, local air quality reports, and the measurements of aerosol optical thickness (AOT) and aerosol vertical profiles from the Southern Great Plains (SGP) Atmospheric Radiation Measurements (ARM) site in Oklahoma. Quantitatively, the model-simulated daily mean near-surface dry smoke mass correlates well with $PM_{2.5}$ mass at 34 locations in Texas and with the total carbon mass and nonsoil potassium mass (KNON) at three IMPROVE sites along the smoke pathway (with linear correlation coefficients R = 0.77, 0.74, and 0.69 at the significance level larger than 0.99, respectively). The top-down sensitivity analysis indicates that the total smoke particle emission during the study period is about 1.3 ± 0.2 Tg. The results further indicate that the simulation with a daily smoke emission inventory provides a slightly better correlation with measurements in the downwind region on daily scales but gives an unrealistic diurnal variation of AOT in the smoke source region. This study suggests that the assimilation of emission inventories from geostationary satellites is superior to that of polar orbiting satellites and has important implications for the modeling of air quality in areas influenced by fire-related pollutants from distant sources.

Citation: Wang, J., S. A. Christopher, U. S. Nair, J. S. Reid, E. M. Prins, J. Szykman, and J. L. Hand (2006), Mesoscale modeling of Central American smoke transport to the United States: 1. ''Top-down'' assessment of emission strength and diurnal variation impacts, *J. Geophys. Res.*, *111*, D05S17, doi:10.1029/2005JD006416.

1. Introduction

[2] Central American Biomass Burning (CABB) in the Yucatan Peninsula and Southern Mexico is an important source of anthropogenic aerosol particles in the troposphere [*Crutzen and Andreae*, 1990]. Burning typically occurs during March–May in the tropical dry season, and ends by early June when the rainy season begins [*Crutzen et al.*, 1979]. During 20 April to 21 May 2003, the Central

[1]Department of Atmospheric Science, University of Alabama, Huntsville, Alabama, USA.
[2]Now at Division of Engineering and Applied Science, Harvard University, Cambridge, Massachusetts, USA.
[3]Aerosol and Radiation Modeling Section, Marine Meteorology Division, Naval Research Laboratory, Monterey, California, USA.
[4]Cooperative Institute for Meteorological Satellite Studies, University of Wisconsin, Madison, Wisconsin, USA.
[5]Office of Research and Development, U.S. Environmental Protection Agency, Research Triangle Park, North Carolina, USA.
[6]Now at NASA Langley Research Center, Hampton, Virginia, USA.
[7]Cooperative Institute for Research in the Atmosphere (CIRA), Colorado State University, Fort Collins, Colorado, USA.

0148-0227/06/2005JD006416$09.00

American region was unusually dry, causing many fires to burn out of control [*Levinson and Waple*, 2004]. Under the influence of southerly winds, the emitted smoke pollutants crossed over the Gulf of Mexico and intruded deep into the southeastern United States (SEUS), thousands of kilometers from the source region. According to the Texas Commission on Environmental Quality (TECQ, http://www.tecq.state.tx.us), the transported smoke plumes severely degraded the visibility and air quality in the coastal regions along the Gulf of Mexico, and resulted in the highest mass concentrations of $PM_{2.5}$ (particulate matter with diameter less than 2.5 μm) measured in this area of Texas since the big fire event in May 1998 [*Peppler et al.*, 2000; *Rogers and Bowman*, 2001]. Simulations of smoke transport driven by accurate estimation of CABB smoke emission have important implications for the air quality forecasts and assessments in this region.

[3] In addition to degrading air quality, the long-range transported smoke aerosols also play an important role in the Earth's climate system. Smoke particles, composed of mostly submicron sized organic compounds are efficient at scattering sunlight as well as acting as cloud condensation nuclei [*Reid et al.*, 1998], impacting the atmospheric radiative transfer both directly and indirectly [*Twomey*, 1977; *Penner et al.*, 1992]. In addition, the black carbon in smoke particles strongly absorbs solar radiation [*Jacobson*, 2001], thereby enhancing atmospheric radiative heating rates, causing temperature inversions [*Robock*, 1988] and "evaporating" clouds [*Ackerman et al.*, 2000; *Koren et al.*, 2004]. The radiative impacts of aerosol particles are believed to be one of the largest uncertainties in the global climate models (GCM) [*Intergovernmental Panel on Climate Change*, 2001], and are not well represented in the standard version of current mesoscale models such as the Fifth-Generation Penn State/NCAR Mesoscale Model (MM5) [*Grell et al.*, 1995] or the Regional Atmospheric Modeling Systems version 4.3 (RAMS4.3) [*Harrington and Olsson*, 2001].

[4] To simulate the smoke transport and to accurately represent smoke radiative impacts in numerical models, the smoke emission inventory must first be defined. Satellite instruments, with reliable repeat cycle and large spatial coverage, have been used widely in the last two decades to detect fires and map the columnar aerosol optical thickness (AOT) of smoke [see *Ahern et al.*, 2001, and references therein]. While these satellite AOT and fire products provide critical references for air quality monitoring and estimation of smoke emission, they are limited in describing the aerosol vertical distribution [*Kaufman et al.*, 2002]. Assimilating satellite-based smoke emission inventories into the aerosol transport models is therefore a preferred method in deriving aerosol three-dimensional (3-D) distributions [*Liousse et al.*, 1996; *Tegen et al.*, 1997; *Chin et al.*, 2002; *Park et al.*, 2003; *Uno et al.*, 2003].

[5] The choice of aerosol transport models as well as the treatment of smoke emission in the model primarily depends on the spatiotemporal scales and physical processes of the study of interest. For climate studies, smoke emission inventories are usually estimated on a monthly or seasonal basis from polar-orbiting satellite fire products [*Ito and Penner*, 2004], and used in conjunction with global aerosol transport models [*Liousse et al.*, 1996; *Chin et al.*, 2002; *Park et al.*, 2003]. However, mesoscale modeling and smoke inventories with finer temporal resolution are appropriate for studying air quality and radiative impacts of smoke aerosols on regional scales [*Westphal and Toon*, 1991; *Jacobson*, 1997; *Byun and Ching*, 1999; *Trentmann et al.*, 2002; *Uno et al.*, 2003; *Carmichael et al.*, 2003; *Colarco et al.*, 2004]. This study is the first in a two-part series and focuses on the mesoscale simulation of CABB smoke transport in the year 2003. The mesoscale model we use is a modified version of RAMS4.3 with the added capability of Assimilation and Radiation Online Modeling of Aerosols (AROMA) [*Wang et al.*, 2004]. The impact of smoke on radiative processes, surface energetics and other atmospheric processes will be presented in part 2 of this series.

[6] Since air quality and radiative impacts of smoke aerosols are highly dependent on the total amount of emitted smoke, the accuracy and availability of the smoke emission inventory are both important for realistically specifying the temporally varying smoke emissions in the numerical model. The accuracy of satellite-derived smoke emission inventory is affected by many highly uncertain variables (i.e., inaccurate emission factors and unknown fire numbers in the absence of satellite observation), and is usually evaluated indirectly by comparing the model-simulated smoke (or carbon) concentration with ground-based observations (so called "top-down" method). For example, *Park et al.* [2003] adjusted the satellite-based smoke emission in their model until the best agreement was achieved between modeled and measured carbon at various observation sites operated by the Interagency Monitoring of Protected Visual Environments (IMPROVE) program [*Malm et al.*, 1994]. However, because their studies used a monthly smoke emission database, the impact of day-to-day variations in smoke emission on the model simulation and emission uncertainty analysis is not clear. In trying to resolve the impact of day-to-day variability of fires on the modeling of carbon monoxide (CO) from the Asian outflow, *Heald et al.* [2003] used CO emission inventories with daily resolution, and showed limited improvement when compared to the modeling results using monthly averaged emission inventories. They attributed this predicament to the dynamical averaging effect during the long-range transport of CO.

[7] Traditional methods of using constant smoke emission rates derived from daily or monthly smoke emission inventories may not be suitable for the simulation of CABB smoke episodes, since biomass burnings in the tropics usually exhibit a pronounced diurnal cycle with peak emissions during early afternoon and minimum emissions at night [*Prins et al.*, 1998]. If meteorological conditions are favorable, the burning will usually start around 1000 local time (LT), and reach its peak around 1200–1400 LT [*Kauffman et al.*, 2003]. As a result, large values of smoke AOT are usually observed during late afternoon and evening [*Reid et al.*, 1999; *Eck et al.*, 2003]. To date, a realistic modeling of such diurnal variation of smoke AOT has not been reported in any numerical simulations that use daily or monthly smoke inventories [*Liousse et al.*, 1996; *Tegen et al.*, 1997; *Chin et al.*, 2002; *Park et al.*, 2003; *Myhre et al.*, 2003].

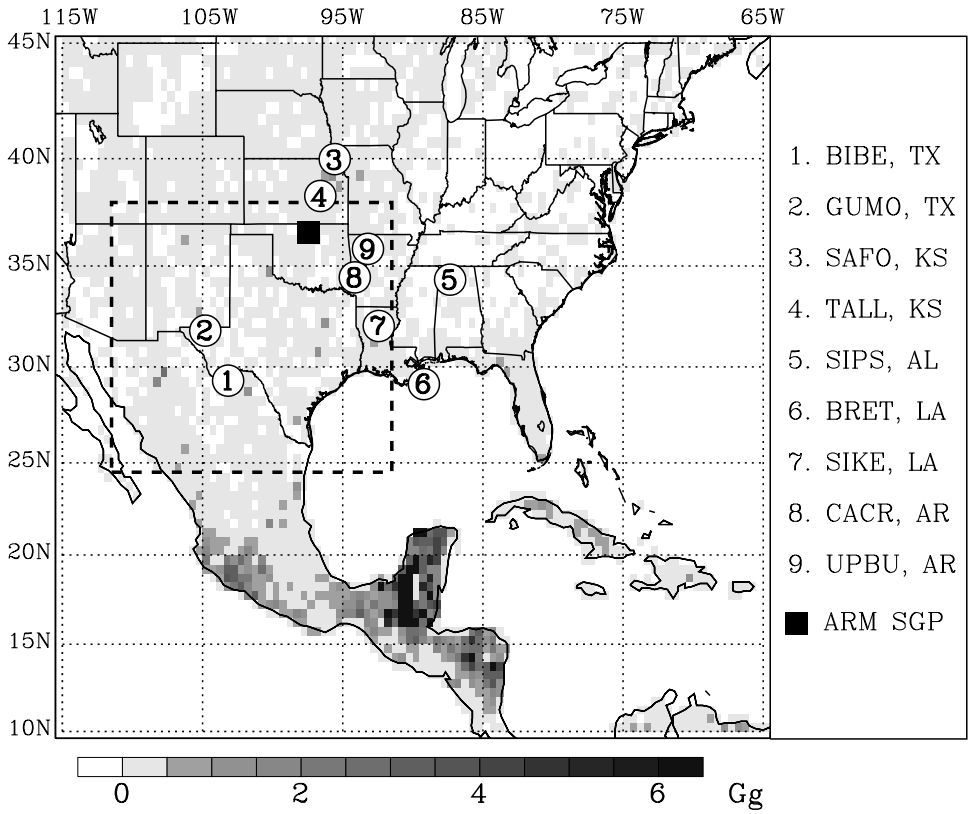

Figure 1. Model domain where the rectangle with dotted lines shows the domain of fine grid. Also overlaid is the map of gray-coded total smoke emission (1 Gg = 10^9 g) from FLAMBE database during 20 April to 21 May 2003. The solid square denotes location of ARM Southern Great Plains (SGP) site, and open circles with different numbers represent the locations of the nine IMPROVE sites (see Table 1 for details).

[8] This study examines the impact of including diurnal variations of fire behavior on smoke transport simulated by RAMS-AROMA. The diurnal fire behavior is specified in the model by using an hourly smoke emission inventory from the Fire Locating and Modeling of Burning Emissions (FLAMBE) geostationary satellite database [*Reid et al.*, 2004] (http://www.nrlmry.navy.mil/flambe/) that in turn utilizes the Geostationary Operational Environmental Satellite (GOES) Wild Fire Automated Biomass Burning Algorithm (WF-ABBA) fire product [*Prins et al.*, 1998]. Compared to a polar-orbiting satellite with a twice-daily revisit time near the equator, GOES WF-ABBA fire observations with a temporal frequency of 30 minutes have the capability to capture diurnal variations of biomass-burning fires [*Prins et al.*, 1998]. We use the top-down approach to evaluate the FLAMBE emission uncertainties by comparing the atmospheric smoke mass concentration simulated by RAMS-AROMA to the ground-based observations. A brief description of these observation data sets and the FLAMBE smoke emission data is presented in section 2. Section 3 describes the RAMS-AROMA configuration and the experimental design of this study. An overview of the smoke events and the model simulation using the FLAMBE smoke emission values (hereinafter referred to as the baseline simulation) are presented in the section 4. Top-down sensitivity analyses of smoke emissions (including their strength and diurnal variation impact) are presented in section 5. Finally, sections 6 and 7 provide the discussion and conclusion, respectively.

2. Data and Area of Study

[9] The area of interest in this study includes the SEUS, Mexico and the Central American region extending to the northern borders of Costa Rica (Figure 1). The data sets used in this study include (1) hourly smoke emissions from FLAMBE, (2) hourly $PM_{2.5}$ mass from the U.S. EPA Aerometric Information Retrieval System Monitoring (AIRS) network, (3) aerosol chemical composition data collected by IMPROVE [*Malm et al.*, 1994], and (4) the AOT data and lidar aerosol extinction profile measured at the Atmospheric Radiation Measurement (ARM) Central Facility (36.6°N, 97.5°W) in the Southern Great Plains (SGP) during the intensive observation period (IOP) in May 2003 [*Schmid et al.*, 2006].

2.1. Hourly Smoke Emission Data

[10] Thirty-minute smoke emission data from the FLAMBE database is used in a one-hour product to specify temporally varying smoke sources in RAMS-AROMA. FLAMBE estimates smoke particle emission inventory using the emission factors outlined by *Ferek et al.* [1998] and the fire products from WF-ABBA, a dynamical contextual multispectral threshold algorithm that identifies fire

pixels and estimates instantaneous subpixel fire size and temperature from GOES multispectral data [*Prins et al.*, 1998]. A detailed description of the FLAMBE algorithm is given by *Reid et al.* [2004, 2005a] and can also be found in online documentation at http://www.nrlmry.navy.mil/flambe/. Currently both the WF-ABBA and FLAMBE system are quasi-operational, with fire location, instantaneous estimates of fire size, and smoke emission flux (kg m^{-2}) generated in near real time for the Western Hemisphere [*Reid et al.*, 2004] (http://www.nrlmry.navy.mil/flambe/).

[11] The distribution of total smoke emitted during the time period of 20 April to 21 May 2003 shows the major emission sources located in the Yucatan Peninsula and the Manzanillo region (18°N, 103°W) in southern Mexico (Figure 1). In the FLAMBE database, the total smoke emission in April and May of 2003 in Central America and Southern Mexico (9–25°N; 120–75°W) were 0.51 Tg (1 Tg = 10^{12} g) and 0.53 Tg, respectively, and the emission during 20 April to 21 May 2003 was 0.75 Tg (as shown in Figure 1). This is the best a priori estimate of the smoke emission in the study region during this time period, and therefore is considered as a baseline emission in the model simulation. In the top-down analysis, the baseline emission is then adjusted by various factors until a best agreement can be found between the simulation and the observation (section 5.1). In order to derive a reasonable range for such adjustment, we first compare the baseline emission data against previous estimates in the same region but in different years.

[12] *Park et al.* [2003] showed that the best estimates of carbon emission in the same region in April and May 1998, were 0.85 Tg and 1.7 Tg, respectively. These estimates are equivalent to 1.2–1.7 Tg and 2.4–3.4 Tg smoke particle emission, assuming carbon mass is about 50–70% of the total smoke particle mass [*Reid et al.*, 2005a, and references therein]. *Hao and Liu* [1994, hereinafter referred to as HL94] estimated that the amount of the dry biomass burned by fires in this region was 39.2 Tg in each April of the late 1970s. Assuming the same emission factor (16 g of carbon per kg dry mass burned) as *Park et al.* [2003], the estimate by HL94 is equivalent to a total of 0.63 Tg carbon. The rate of deforestation in this region is estimated to have increased 0.5% per year in the 1980s and 1.2% per year from 1990 to 1995 [*Food and Agricultural Organization*, 1997]. Using these deforestation rates and the same carbon/particle mass ratio to extrapolate HL94's values, it is expected that CABB smoke particle emission should be at least 1.1–1.5 Tg in a normal April for years after 1995. The extrapolated values and the estimates by *Park et al* [2003] are reasonable, because CABB fire events in 1998 are among the largest reported in the literature [*Peppler et al.*, 2000]. The above analysis suggests that the current FLAMBE emission database most likely underestimates the total smoke emission, since the CABB fire events in 2003 caused the largest $PM_{2.5}$ concentration measured in southern Texas since 1998 (TECQ, http://www.tecq.state.tx.us). In the analysis of South American smoke emission, *Reid et al.* [2004] also showed that a 40% underestimate of real smoke emission may exist in the FLAMBE database, because of various nonidealities in the fire products and emission algorithms. To infer the amount of underestimation in the baseline emission, we increase the baseline emission by several factors ranging from 0 up to 100% in the top-down sensitivity analysis (section 5).

2.2. EPA AIRS $PM_{2.5}$ Data and Smoke Coverage Report

[13] The EPA AIRS observation network [*Watson et al.*, 1998] routinely measures the hourly $PM_{2.5}$ mass concentration at more than 1500 stations across the United States. At the majority of stations, mass concentrations are measured near the surface using the Tapered-Element Oscillating Microbalance (TEOM) instruments [*Watson et al.*, 1998]. Particle-bound water included in the sampled air is removed by heating at a constant temperature (usually at 50°C) inside the instrument [*Watson et al.*, 1998]. Such heating procedures, although necessary for the removal of water in the sampled $PM_{2.5}$, can also result in evaporation of semivolatile particulate matter such as volatile organic carbon and ammonium nitrate [*Allen et al.*, 1997]. For this reason, the TEOM may underestimate the $PM_{2.5}$ mass by 1–2 μg m^{-3} for 24 hour averages and may have a larger uncertainty in the hourly $PM_{2.5}$ mass concentration [*Charron et al.*, 2004; *Hitzenberger et al.*, 2004]. *Allen et al.* [1997] have shown that sometimes significant, unrealistic fluctuations in the TEOM $PM_{2.5}$ mass concentration can occur over several hours, because of the change of equilibrium state of particles on the TEOM filter when ambient pollutants or moisture is changing rapidly. Nevertheless, the hourly $PM_{2.5}$ data from the TEOM instrument are sufficient to qualitatively capture the diurnal variations of $PM_{2.5}$ mass and to quantitatively assess the 24 hour-average $PM_{2.5}$ mass.

[14] In addition to the $PM_{2.5}$ mass data sets from the EPA AIRS network, for comparison purposes, the daily reports of smoke coverage area estimated by the TECQ air quality monitoring personnel are also used as a reference. These reports documented the transported CAAB smoke in Texas in April–May 2003, and an estimation of the smoke coverage area was made at 1300 LT every day by using a combination of the ground observations as well as satellite images (http://www.tceq-uation state.tx.us/assets/public/).

2.3. IMPROVE Data

[15] The IMPROVE network was initiated in spring of 1988, and consists of about 165 monitoring sites across the United States [*Malm et al.*, 1994, 2004], of which 9 stations are located in the area of interest for the current study (see Figure 1 and Table 1 for a list of data sets used). At each site, sampling modules are used to collect the $PM_{2.5}$ mass on every *third* day, with a sampling duration time of 24 hours. The collected samples are then analyzed to infer the concentration of $PM_{2.5}$ mass and other trace elements such as potassium (K) and iron (Fe), as well as the major visibility-reducing aerosol species such as sulfates, nitrates, organic compounds, black (light-absorbing) carbon, and wind-blown dust [*Malm et al.*, 1994]. In this study, we use the 24 hour IMPROVE data collected in April–May 2003 for model validation, and monthly averaged IMPROVE data during 2000–2002 to derive the background concentration of carbonaceous aerosols (section 5.1).

Table 1. Location and Site Names of Nine IMPROVE Monitoring Stations

Site Name	Location	Latitude, °N	Longitude, °W
BIBE	Big Band National Park, Texas	29.30	103.12
GUMO	Guadalupe Mountains, Texas	31.83	104.81
SAFO	Sac and Fox, Kansas	39.98	95.57
TALL	Tallgrass, Kansas	38.30	96.60
SIPS	Sipsy Wilderness, Alabama	34.34	87.34
BRET	Brenton, Louisiana	29.12	89.21
SIKE	Sikes, Louisiana	32.06	92.43
CACR	Caney Creek, Arkansas	34.45	94.14
UPBC	Upper Buffalo Wilderness, Arkansas	35.83	93.20

[16] Of particular interest is the organic carbon (OC) and black carbon (BC) concentrations as well as nonsoil particulate potassium (K) from smoke measured at the various IMPROVE sites in SEUS, because these species are tracers of the smoke particles originating from biomass burning [*Kreidenweis et al.*, 2001]. IMPROVE uses the thermal optical reflectance (TOR) method to analyze the concentration of OC and BC [*Chow et al.*, 1993; *Malm et al.*, 1994]. Similar to other methods of measuring OC and BC, the TOR method has uncertainties from both analytical sources and artifacts [*Chow et al.*, 1993]. The uncertainty is estimated to be 15% for OC and 18% for BC, and sometimes can be up to 50% [*Chow et al.*, 1993]. Although accurate separation of BC and OC is difficult, less uncertainty (7∼9%) is associated with the derived total carbon (OC + BC) concentration [*Schmid et al.*, 2001], and so only the total carbon mass (OC + BC) is used in this study.

[17] Nonsoil potassium in smoke particles is another indicator of biomass burning aerosols [*Kreidenweis et al.*, 2001]. *Tanner et al.* [2001] showed that during Central American fire events in May 1998, the K concentration in the SEUS exceeded 300% of normal mean value. However, the sources of K in the atmosphere include not only smoke but also soil. In this study, the technique of *Kreidenweis et al.* [2001] is used to estimate the mass of smoke K from nonsoil sources (referred to as KNON, and is equal to total mass of K minus 60% mass of Fe). The derived KNON data from the IMPROVE measurements are used to validate the smoke simulation from the model.

2.4. AOT and Lidar Data at the ARM SGP Site

[18] AOT data inferred from the normal incidence multifilter radiometer (NIMFR) in the ARM SGP site (solid square in Figure 1) during May 2003 are used to intercompare with model simulations. The NIMFR measures the direct solar radiation at 5 wavelengths centered at 415, 500, 615, 673, and 870 nm. AOTs are calculated on the basis of the Beer-Lambert-Bouguer law. The calculation also includes a correction for Rayleigh scattering and ozone optical thickness. The AOT data available from the ARM data archive (http://www.archive.arm.gov/) are quality controlled with an uncertainty between 0.01 and 0.02.

[19] The aerosol profiles retrieved from a Raman lidar operating at the ARM SGP site [*Ferrare et al.*, 2006] are used to compare against the modeled smoke profiles. The Raman lidar measures backscattered light at the laser wavelength of 355 nm as well as the water vapor and nitrogen Raman shifted returns at 408 nm and 387 nm, respectively. The Raman technique uses the Raman nitrogen signals, and therefore has advantages in deriving the aerosol extinction (km^{-1}) profiles without making an assumption about the lidar backscatter ratio and without using AOT as a constraint [*Ferrare et al.*, 2001]. Unfortunately, it was recently found that the sensitivity of Raman lidar at the ARM site has experienced a gradual loss since 2001 [*Ferrare et al.*, 2006]. Hence the Raman lidar derived aerosol extinction profile is only used qualitatively in this study to identify the location of smoke layers.

3. Model Description

[20] The RAMS-AROMA model [*Wang et al.*, 2004] is a modified version of the standard RAMS4.3 model [*Pielke et al.*, 1992] with added capabilities of modeling aerosol transport and a new radiative transfer scheme that explicitly accounts for the aerosol radiative impacts. Since the aerosol transport model in RAMS-AROMA directly utilizes the tracer advection scheme in RAMS, it can produce with higher temporal resolution the 3-D distribution of aerosols than the offline aerosol transport models. In addition, the online transport simulation also avoids possible time lag, mismatch, and repeated computations that could occur between the offline aerosol transport and its external meteorological data sources. Since the standard version of RAMS4.3 only considers the cloud radiative effects, we replaced the original RTM [*Harrington and Olsson*, 2001] in RAMS4.3 with an updated version of a δ-4 stream plane-parallel broadband radiative transfer model (RTM) originally developed by *Fu and Liou* [1993] to take into account the radiative impacts of both aerosol and clouds during the model simulation [*Wang et al.*, 2004]. With this design, the aerosol radiative impacts are directly tied into the simulated physical processes in the atmosphere, allowing the dynamical processes in the model to impact aerosol transport and vice versa.

[21] The RAMS-AROMA model, initially developed by *Wang et al.* [2004] to assimilate the GOES-derived AOT for the dust simulation in the Puerto Rico Dust Experiment (PRIDE), is modified in this study to assimilate a satellite-derived smoke emission inventory and to simulate the long-range transport of CABB smoke aerosols (section 3.1). During the simulation, smoke AOT is computed (section 3.2) and the smoke radiative impacts are taken into account at each model step. The different model experiments are then designed to investigate the smoke emission uncertainties and the impacts of diurnal

variations in smoke emissions on the model simulation (section 3.3).

3.1. Smoke Transport and Assimilation of Smoke Emission

[22] Smoke particles can undergo various processes such as condensation, coagulation, dispersion, advection, and activation (as cloud condensation nuclei) before they are removed from the atmosphere through dry and wet deposition [*Reid et al.*, 2005a]. Since smoke plumes contain hundreds of organic compounds whose individual composition and formation mechanisms are not well understood [*Turpin et al.*, 2000], the evolution of smoke physical and chemical properties are still not clear [*Gao et al.*, 2003]. What has been recognized is the rapid change of smoke properties in the first ~30 min to 1 hour after the emission [*Reid and Hobbs*, 1998; *Reid et al.*, 1998], a period in which the young smoke particles dilute rapidly from a high-temperature environment into the cooler ambient atmosphere, and thus condensation and coagulation processes are expected to occur favorably [*Hobbs et al.*, 2003]. If meteorological conditions allow, regional haze composed of aged smoke particles from different individual fires can be transported long distances to the downwind areas. During transport, the evolution of smoke particles continues through formation of secondary organic aerosol particles (e.g., photochemical production and gas-to-particle conversion), oxidation of hydrocarbon compounds, as well as condensation of organic and inorganic species on the smoke particles [*Reid et al.*, 2005a].

[23] Numerical modeling of the smoke aging process immediately after the emission [e.g., *Turco and Yu*, 1999] as well as the formation of secondary organic aerosols (SOA) in the atmosphere [e.g., *Strader et al.*, 1999; *Schell et al.*, 2001] demonstrate the need for further improvement in the models (see review by *Kanakidou et al.* [2005]). The global and annual SOA formation estimates vary by almost a factor of 6 in different CTMs, partially because of the lack of detailed and consistent treatment of the relevant chemical mechanisms (such as gas-particle portioning) [*Pun et al.*, 2003] and the large uncertainties (a factor of 2–5) in the estimates of SOA precursor emissions [*Kanakidou et al.*, 2005]. In regional scale, several case studies have demonstrated the success of SOA simulation [*Jacobson*, 1997; *Zhang et al.*, 2004]. However, the initialization of these models requires the detailed and accurate chemical speciation data (such as SOA precursor emissions) that can only be possible through extensive measurements [*Jacobson*, 1997; *Zhang et al.*, 2004]. Indeed, direct measurements of SOAs are needed, and the current estimation of SOA relies mostly on indirect methods that are highly uncertain (see discussion by *Yu et al.* [2004]). Furthermore, since smoke aging processes depend strongly on the biomass burning characteristics (e.g., flaming, smoldering, fuel types, etc.) and ambient meteorology of individual fires [*Reid and Hobbs*, 1998; *Hobbs et al.*, 2003], it remains a challenging task to consider the aging process of smoke particles from thousands of individual fires in the Eulerian models (such as RAMS) operating on synoptic spatial scales. Therefore RAMS-AROMA assumes that the satellite-derived smoke emissions represent aged smoke particles and hence neglects the SOA formation and smoke aging process in the model. This assumption is similar to those made in other aerosol transport models [*Westphal and Toon*, 1991; *Liousse et al.*, 1996; *Chin et al.*, 2002; *Park et al.*, 2003; *Uno et al.*, 2003]. A multiyear analysis of IMPROVE data will be used in the top-down analysis of smoke emissions to evaluate possible model uncertainties due to the lack of SOA formation in the model (section 5.1).

[24] By neglecting SOA formation and chemical processes associated with smoke aging, the change of local smoke mass concentration is mainly due to such processes as transport, emission, dry deposition, and wet deposition:

$$\frac{\partial C}{\partial t} = \left(\frac{\partial C}{\partial t}\right)_{transport} + \left(\frac{\partial C}{\partial t}\right)_{emission} + \left(\frac{\partial C}{\partial t}\right)_{dry-deposition} + \left(\frac{\partial C}{\partial t}\right)_{wet-deposition} \quad (1)$$

In AROMA, the transport term is implemented using the generalized scalar advection framework available in RAMS [*Wang et al.*, 2004]. In addition to the dry deposition by *Slinn and Slinn* [1980] over the ocean surface already present in RAMS-AROMA [*Wang et al.*, 2004], modifications have been made to include a dry deposition scheme over the land [*Zhang et al.*, 2001] and a wet-deposition scheme for both washout [*Slinn*, 1984] and rainout processes [*Pruppacher and Klett*, 1978]. Both dry deposition schemes include effects of gravitational settling, Brownian diffusion, and surface characteristics (surface roughness length and radius of collectors as a function of surface type and season). In the two wet deposition schemes, the deposition velocity is parameterized as a function of rain rate in the model. The smoke emission rate within a grid cell of area A (m^2) is calculated as:

$$\left(\frac{\partial C}{\partial t}\right)_{emission} = \frac{\sum_j F_j \bullet S_j}{A \bullet H \bullet \Delta t} \quad (2)$$

where j represents jth fire within that grid; F and S are the smoke emission flux (kg m^{-2}) and fire size (m^2), respectively, both specified using the FLAMBE data set; H is the injection height (m), and the smoke particles are well mixed in all model layers below this height. Since hourly smoke emission is used, Δt is set to 1 hour.

[25] It is a common practice in aerosol transport models to uniformly distribute the smoke aerosols within H so that the buoyancy caused by the heat from fires can be taken into account [*Colarco et al.*, 2004]. However, there is no consensus on the method of defining H in the model. Prior studies suggest various values of H that ranging from 2 km in global CTMs [*Liousse et al.*, 1996; *Forster et al.*, 2001; *Davison et al.*, 2004] to 5–8 km in regional simulations of smoke from intensive Canadian fires [*Westphal and Toon*, 1991; *Colarco et al.*, 2004]. On the basis of the observations from different field experiments, *Lavoue et al.* [2000] found that typical injection height generally follows a linear relationship (with correlation coefficient of 0.95) with the fireline intensity (I, in unit of kW m^{-1}):

$$H = a \bullet I \quad (3)$$

where $a = 0.23$ m^2 kW^{-1}. They further showed that H is usually about 2–3 km for fires in northern latitudes (such as over Russia), but Canadian intensive "crown" fires usually have a mean I of 33,000 kW m^{-1}, which render a mean injection height up to 7–8 km.

[26] The biomass burning in Central America is usually less intensive than boreal forest fires, because individual farmers ignite most fires for agricultural purposes [*Kauffman et al.*, 2003]. Indeed, the trees are first slashed and useful wood products are removed by farmers before they are ignited [*Kauffman et al.*, 2003]. As a result, the fireline intensity I of CABB fires is only in the range ~4000–7800 kW m^{-1} [*Kauffman et al.*, 2003], which, on the basis of equation (3), implies that the injection height H is ~0.9–1.5 km. Therefore we set H at the eighth layer (about 1.2 km) in the model. Sensitivity studies are carried out to examine the impact of injection height on the simulation results (section 5.2).

3.2. Modeling of Smoke Optical Properties

[27] Smoke optical properties including mass extinction coefficient, single scattering albedo, and asymmetry factor are needed in the RAMS-AROMA to derive the smoke AOT and extinction profile from the smoke mass concentration and to compute the smoke radiative effects. In RAMS-AROMA, the smoke AOT is calculated using:

$$\tau = \sum_{i=1}^{K} (Q_i \times C_i \times f(rh_i)) \times \Delta z_i \qquad (4)$$

where i denotes the index for the vertical layers, K is the total number of layers in the model, C is the aerosol mass concentration (g m^{-3}), Q is the mass extinction efficiency (m^2 g^{-1}), Δz is the layer thickness (m) and $f(rh)$ is the hygroscopic factor expressed in RAMS-AROMA as a function of relative humidity (rh) described by *Kotchenruther and Hobbs* [1998]. Smoke optical properties in RAMS-AROMA are adapted from *Christopher and Zhang* [2002], and are based on Mie theory computations in which the size distribution and refractive index of smoke aerosols derived during the Smoke, Cloud and Radiation–Brazil (SCAR-B) experiment are used. The computed Q of dry smoke aerosols is approximately 4.5 m^2 g^{-1} at 550 nm. Although this value is consistent with the lower end of Q reported in the literature (see review paper by *Reid et al.* [2005b]), an underestimation of 30% is possible. A Q value of 5 m^2 g^{-1} was used by *Penner et al.* [1992] in the box model estimation of global smoke radiative forcing at TOA. Recent studies also reported that the CABB smoke aerosols might have larger hygroscopicity than southern American smoke aerosols [*Kreidenweis et al.*, 2001; *Iziomon and Lohmann*, 2003] This uncertainty of Q is considered in the analysis of our model results (section 5.1).

3.3. Experiment Design

[28] A nested grid configuration is used in this study, with a fine grid of 62 × 62 points and 30 km grid spacing covering Texas, nested within a coarse grid with 48 × 48 grid points and 120 km grid spacing (Figure 1). Both horizontal grids use a stretched vertical grid of 30 points and grid stretch ratio of 1.2, with the vertical grid spacing increasing from 50 m near the surface to a maximum of 750 m higher in the atmosphere. The National Center for Environmental Prediction (NCEP) reanalysis data [*Kalnay et al.*, 1996] at 0000, 0600, 1200 and 1800 UTC are used for initializing and specifying the temporally evolving lateral boundary conditions. In RAMS-AROMA, we select the Kuo's cumulus cloud parameterization to represent the subgrid-scale cumulus convection [*Walko et al.*, 1995]. The level 2.5 turbulent closure model [*Mellor and Yamada*, 1974] and Land Ecosystem Atmosphere Feedback module [*Walko et al.*, 2000] are used to simulate the boundary diffusion process and air-surface interaction, respectively. Since we are only interested in the CABB smoke particles, the background aerosols and the transport of aerosols from outside the model boundary are not included.

[29] Six different simulations are considered in this study and they differ only in the treatment of biomass-burning emissions and injection height. Experiment A (section 4) uses the hourly FLAMBE baseline emissions and sets the eighth model layer as the injection height (hereinafter will be referred as Layer8-Hourly-1.0E simulation, or simply baseline simulation). This baseline emission inventory is also used in the NRL Aerosol Analysis and Prediction System (NAAPS) operational aerosol forecast model (http://www.nrlmry.navy.mil/aerosol/), but with a 6-hour temporal resolution. In experiments B and C (section 5.1), FLAMBE emissions are increased (through scaling the emission in each hour) by 50 and 100%, respectively (hereinafter will be referred as Layer8-Hourly-1.5E and Layer8-Hourly-2.0E). Experiment D (section 5.2) uses the daily emissions derived from hourly FLAMBE baseline emissions to examine the impact of diurnal emissions on the smoke transport (hereinafter Layer8-Daily-1.0E). The daily smoke emission is constructed by merging all (24) hourly baseline emission on a given day, and the emission rate is calculated similarly to equation (2), except that Δt is set as 24 hours. Experiments E and F are similar to the baseline experiment, but the injection height is set at the seventh (ΔH ~ 1.0 km) and ninth model layer (ΔH ~ 1.4 km), respectively (hereinafter Layer7-Hourly-1.0E and Layer9-Hourly-1.0E). All numerical experiments are initiated at 1200 UTC on 20 April 2003 and end at 1200 UTC on 21 May 2003.

4. Results in the Baseline Simulation

4.1. Overview and Qualitative Analysis

[30] The $PM_{2.5}$ mass measurements at various stations in Texas during 21 April to 21 May 2003 indicate that the air quality in southern (Figures 2a and 2b), central (Figures 2c–2e), and eastern Texas (Figure 2f) were severely degraded by the smoke events and the air quality categories ranged from moderate to unhealthy. Particularly, the air quality in southern Texas was affected by CABB smoke events almost everyday during the 30-day time period (Figures 2a and 2b). The $PM_{2.5}$ mass variations shown in Figure 2 illustrate that there were four major smoke events during the following time frames: 21–26 April, 27 April to 12 May, 13–17 May, and 18–21 May, respectively. In the second event, the $PM_{2.5}$ mass concentration started to increase on 27 April and reached the peak during 8–10 May at almost all stations except those in the western and northern parts of Texas

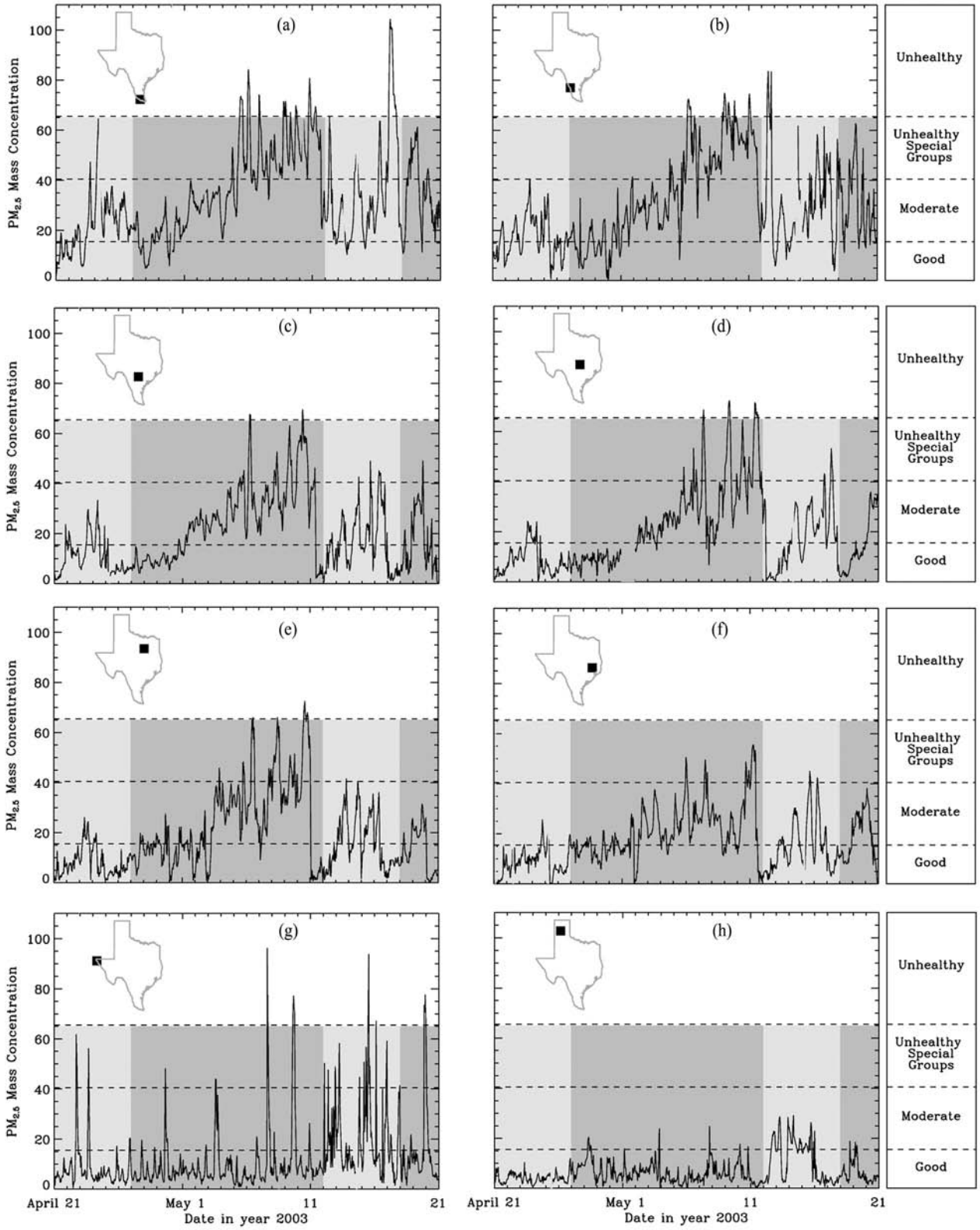

Figure 2. Time series of $PM_{2.5}$ mass concentration in various ground-based stations in the state of Texas. The inset map in each panel shows the location of the corresponding station in Texas. The horizontal dotted lines in each panel outline the air quality categories based on the EPA 24-hour standard; for example, $PM_{2.5}$ mass (in μgm^{-3}) of 15.4, 40.4, 65.4, 150.4, 250.4, and 500.4 are upper limits for the categories of good, moderate, unhealthy for special groups (e.g., elderly and children), unhealthy, very unhealthy, and hazardous, respectively. The shaded background in different time intervals highlights the time frames of four major smoke events (see text for details).

(Figures 2g and 2h). $PM_{2.5}$ mass concentrations in southern and central Texas stations (Figures 2a–2f) suddenly dropped by a factor of about 2–3 on 12 May, a clear sign of cessation of the 15-day smoke pollution event. The events on 8–10 May were the most severe, resulting in unhealthy air quality at most stations. Satellite images during this time period indicate large smoke plumes were continuously transported across the Gulf of Mexico, impacting the SEUS (Figures 3a and 3b).

[31] Note that CABB smoke was not observed at all stations in Texas. There was apparently less smoke (if any) being transported to the western part of Texas, as the timeline of $PM_{2.5}$ mass in this region demonstrated (Figure 2g) little consistency with that in other stations (Figures 2a–2f). The sharp spikes of $PM_{2.5}$ mass concentration in Figure 2g spanned relatively short time intervals ranging from 1 to 2 hours and were possibly caused by local emission sources. The influence of smoke events was also not obvious in the station located in northern Texas (Figure 2h) except on 12–18 May when an increase in $PM_{2.5}$ mass concentrations was consistent with other stations. The area most frequently covered by smoke during this 30-day time period include the southern, central and eastern part of Texas, as well as nearby areas in Louisiana, Arkansas and Oklahoma [*Peppler et al.*, 2000]. Hereinafter these areas are referred as the smoke pathway regions.

[32] The RAMS-AROMA simulation of the largest CABB smoke episode that occurred during 9–12 May 2003 is depicted in Figures 3e–3h, respectively. A stable high-pressure system was centered over Florida from 9 to 10 May, building a ridge along 85°W north to 35°N (Figures 3e and 3f). Southeasterly winds in the lower troposphere associated with this system continuously transported smoke aerosols from the source regions over the Yucatan Peninsula to Texas and other parts of the SEUS, which was also observed in the satellite images (Figures 3a and 3b). In the midlatitude region (35°N–40°N), the smoke plumes were moved eastward by the prevalent westerly flow. These optimal meteorological conditions resulted in the smoke front reaching West Virginia on 10 May (Figure 3f). The northern part of the ridge started to move eastward on 11 May (Figure 3g). A low-pressure system originally centered at 45°N, 103°W on 9 May (Figure 3e) moved in on 10 May, and replaced the ridge on 12 May (Figure 3h). These synoptic changes shifted the winds from southeasterly flow (Figures 3e and 3f) to mainly westerly (Figure 3g) and northwesterly flow (Figure 3h) between 35 and 40°N, resulting in the retreat of smoke fronts on 11 and 12 May. The clouds associated with the low-pressure system made such retreat invisible in the satellite images over the continental United States (Figure 3c). However, this retreat can still be seen in Figure 3d that showed the majority of smoke plumes were in the southern part of the Gulf of Mexico. Overall, the model-simulated spatial distribution of smoke plumes (Figures 3e–3h) over the ocean is in a good agreement with those in the satellite images (Figures 3a–3d).

[33] Assuming that the occurrence of moderate to worse air quality over large contiguous areas is an indicator of large-scale aerosol events, the model performance is qualitatively evaluated by comparing simulations to air quality categories at various AIRS $PM_{2.5}$ stations. On 9 and 10 May, the baseline simulation indicates that the air quality in Texas, Arkansas, Kentucky and West Virginia were affected by the smoke (Figures 3e and 3f), consistent with the moderate to unhealthy air quality category (e.g., AIRS $PM_{2.5}$ mass > 15.5 $\mu g\ m^{-3}$) reported by the majority of the stations (88%) in these regions. On 11–12 May, observations showed that except for the southern part of Texas, air quality in the majority of the SEUS was good, indicating that these regions were not affected by CABB smoke. These features are also well simulated by the model (Figures 3g and 3h), particularly in the Texas region where the areas with modeled high smoke concentration match well with the polluted area estimated by the TECQ (denoted by red curves in Figure 3). It should be emphasized that the smoke coverages estimated by TECQ are mainly based upon ground-based measurements and local reports in Texas and nearby regions. Therefore the red curves only extended to 37°N, and did not cover the northeastern states such as West Virginia, albeit these regions were affected by smoke plumes (Figures 3e and 3f). Note that $PM_{2.5}$ mass measurements showed moderate air quality in New Jersey on 10 May (Figures 3e and 3f) that may potentially be related to a local emission sources that is not resolved by the current version of RAMS-AROMA.

[34] The performance of RAMS-AROMA is further evaluated by comparing model-simulated vertical distribution of smoke to lidar-derived aerosol extinction profiles from the ARM SGP site during 9–11 May 2003. At 0000 UTC on 9 May 2003 (local time is 5 hours behind UTC), the lidar measurements showed that the smoke layer was located in a shallow PBL within 700 m above the surface (Figure 4a). Around midnight (0500 UTC), the nocturnal PBL demarcated the residual layer and eventually became a 100-m shallow layer near the surface in the early morning (1200 UTC, 9 May), and the smoke concentration decreased during this time period (Figure 4a). The PBL height rose and reached about 1km in late morning (1500 UTC) on 9 May. Associated with the increase in PBL height was the transport of smoke that enhanced the smoke concentration in the PBL. An upper level (3–4 km above the surface) smoke layer moved into the ARM site and was entrained together with the PBL in the late afternoon (2000 UTC). At night, the PBL height decreased. High concentrations of smoke were found in the shallow PBL from 0600 UTC to 1500 UTC on the late morning of 10 May (Figure 4b), and a residual layer with low smoke concentrations can be seen from 0300 UTC to 1500 UTC on 10 May. The smoke concentrations decreased and totally disappeared on 11 May (Figure 4c). The model (Figures 4d–4f) successfully captured the relative locations of each smoke layer as well as their diurnal evolution shown in Figures 4d–4f, particularly the evolution of smoke profiles from 0000 to 1500 UTC on both 9 and 10 May, and the cessation of smoke plumes on 11 May. However, because of the temporal (hourly) and spatial resolution (30×30 km^2 and 18 vertical layers) of the model output used in the Figures 4d–4f, the model results are unable to resolve the subgrid fine structures shown in Figures 4a–4c. In addition, the Rayleigh and Mie scattering of background aerosols could also be important at 335 nm, thus some variations in the lidar-

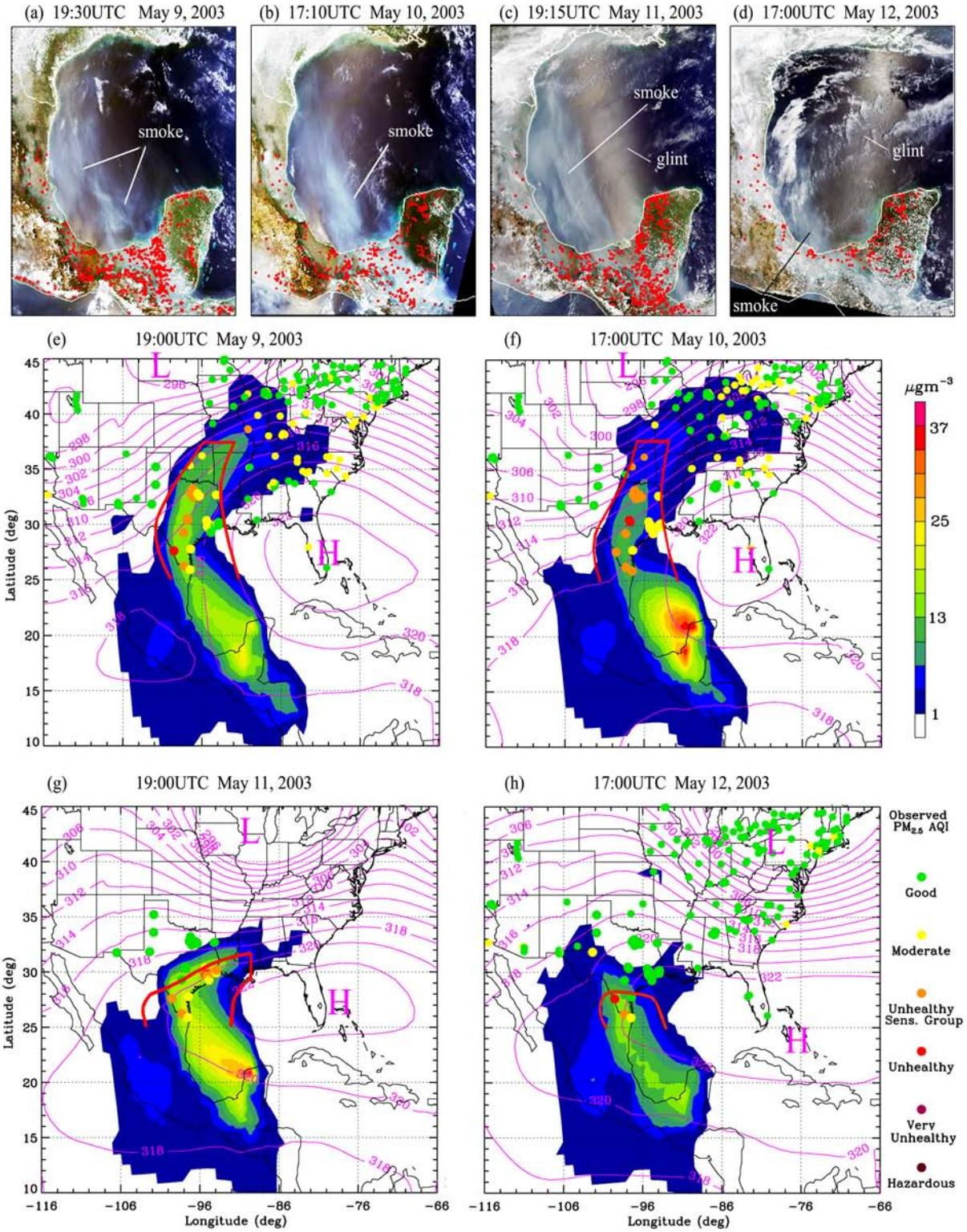

Figure 3. (a–d) MODIS three-band color overlay images (red, band 1; green, band 4; and blue, band 3) from Terra and Aqua satellites during 9–12 May 2003 of smoke plumes transiting from Yucatan Peninsula along the Gulf coast of Mexico to the SEUS. Red dots indicate the location of fires detected by MODIS. Sunglint and smoke regions have also been denoted. (e) Modeled dry smoke concentration near the surface on 1800 UTC 9 May 2003. Solid dots show the locations of different $PM_{2.5}$ observation sites and are color-coded on the basis of air quality categories. Red curves show the TECQ best estimate of smoke coverage (see text for details). Pink contour lines are the geopotential heights (in 10 m) at 700 hpa. Letters H and L locate the major high- and low-pressure systems. (f–h) Same as Figure 3e but for 10, 11, and 12 May, respectively. Note in Figure 3g that $PM_{2.5}$ data were only available in Texas.

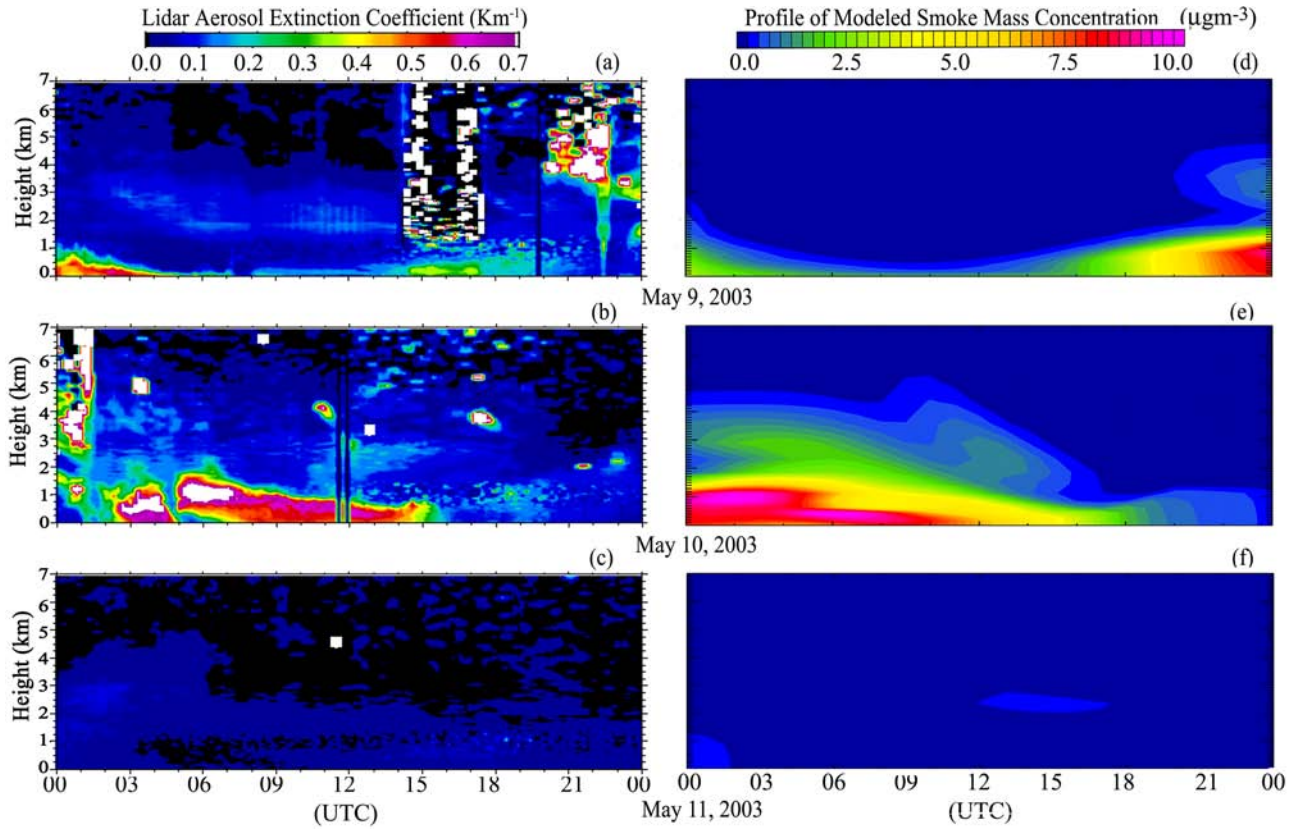

Figure 4. (a–c) Time series of aerosol extinction coefficient (km^{-1}) profiles at 335 nm derived from lidar measurements at ARM SGP site on 9, 10, and 11 May 2003, respectively. (d–f) Same as Figures 4a–4c but showing the profile of modeled smoke mass concentration.

derived aerosol profile (such as low aerosol extinction coefficients at 2–3 km during 0300–1500 UTC of 9 May 2003) may be caused by the inhomogeneous distribution of nonsmoke aerosols.

4.2. Quantitative Analysis of Baseline Simulation

4.2.1. Comparison With $PM_{2.5}$

[35] The spatial distribution of the linear correlation coefficient R between daily averaged model-simulated surface smoke mass concentrations and the daily averaged $PM_{2.5}$ mass concentrations at 36 stations in Texas (Figure 5) shows values ranging between 0.7 and 0.9 for the majority of the stations (23 out of 36). Daily averaged $PM_{2.5}$ mass concentration, one of the EPA's standards in evaluating the daily air quality, is considered in this study rather than the hourly averaged value. The hourly $PM_{2.5}$ mass concentration could be significantly affected by local emissions such as traffic and microscale rapid change in meteorological conditions [*Allen et al.*, 1997], factors not currently resolved in RAMS-AROMA. The daily averaged $PM_{2.5}$ mass is less affected by these factors, and is a reasonable indicator of the smoke particle concentration during the smoke event. Comparison between hourly $PM_{2.5}$ mass and model-simulated smoke mass concentrations indicates a mean R value of 0.55 at the 36 stations in Texas, significantly lower than 0.73 in the daily comparison (figures not shown).

[36] High correlations (>0.7) are generally in the southern (Figures 6b and 6c), central Texas (Figure 6d) and northeastern (Figures 6e–6f) Texas. In the Dallas region (33°N, 97°W), about two third of the stations have R values larger than 0.8. Low correlations exist mainly in western Texas and coastal region, in particular near the Houston area (Figure 5). Since less smoke was transported to western Texas, local emissions dominated the daily averaged

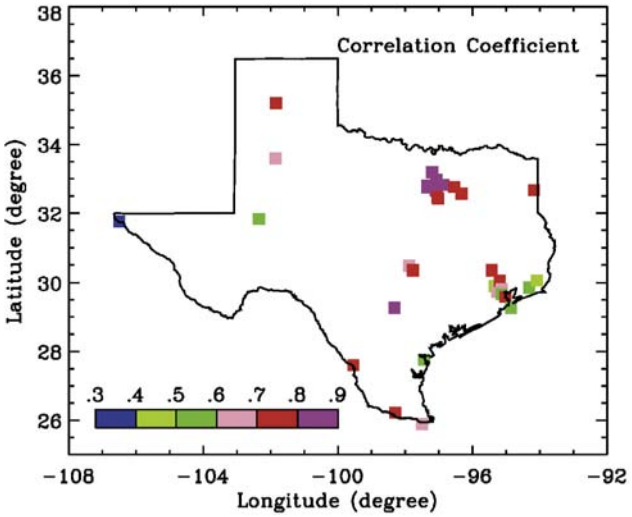

Figure 5. Map of correlation coefficients between daily averaged modeled smoke concentration near the surface with the measured $PM_{2.5}$ concentration at different $PM_{2.5}$ sites in Texas.

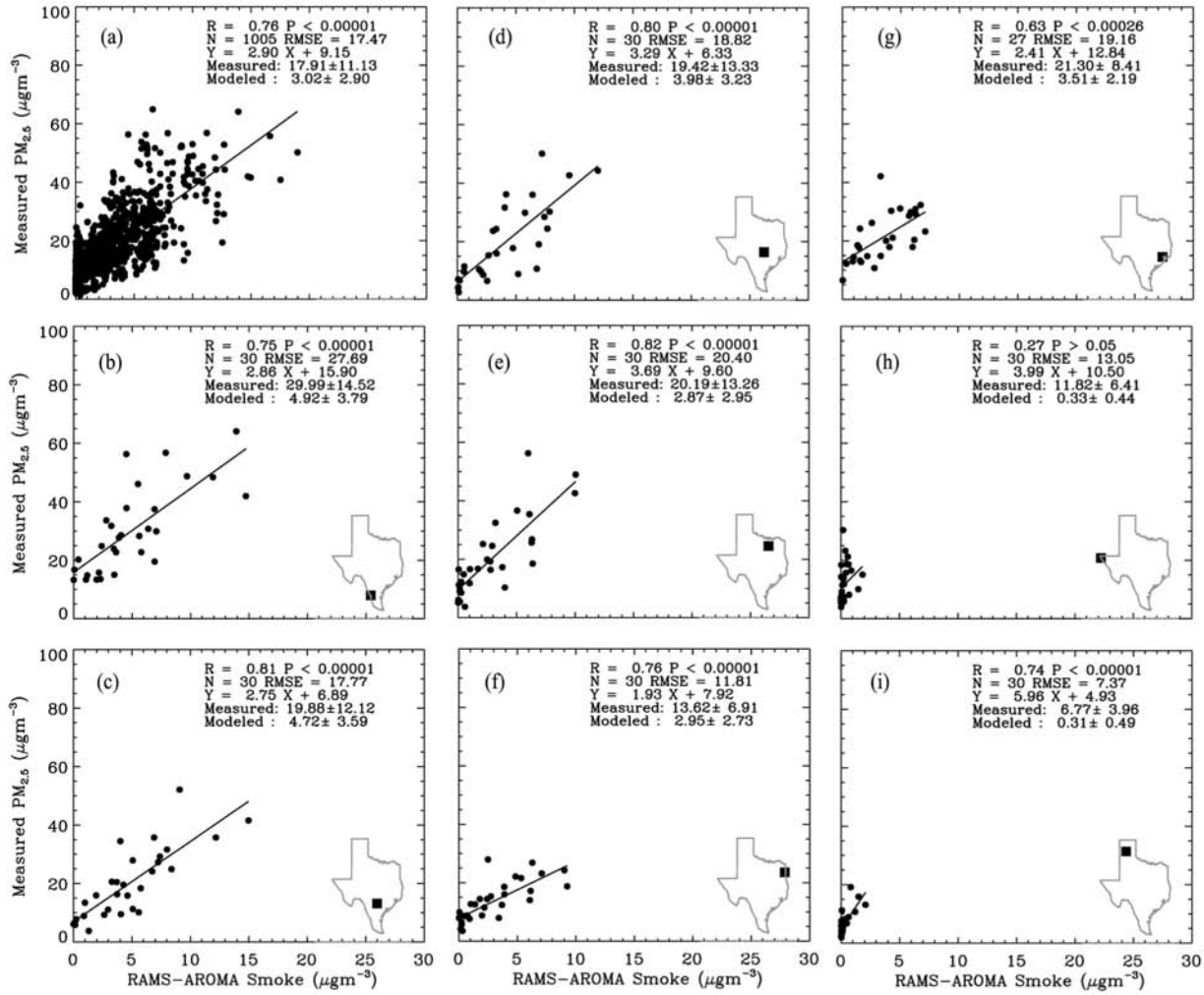

Figure 6. (a) Comparison between daily averaged modeled smoke concentrations (x axis) near the surface with the measured $PM_{2.5}$ concentration (y axis) near the surface at 34 $PM_{2.5}$ observation sites in state of Texas. (b–i) same as Figure 6a but at different individual site (solid square in the inset map). Also shown in each panel are the correlation coefficient (R), the significance level of correlation (P, not significant when P greater than 0.05), number of comparison pairs (N), root mean square error (RMSE), and mean ± standard deviation of both modeled and measured quantities.

$PM_{2.5}$ mass, and hence RAMS-AROMA failed to capture the variations of daily mean $PM_{2.5}$ mass in this region (Figure 6h). In the Houston area, emissions from petrochemical industries in the ''ship channel area'' along the bank of Galveston Bay include significant amounts of hydrocarbons [*Allen*, 2005]. Its large day-to-day variation is a major factor in controlling daily fluctuations of $PM_{2.5}$ mass in the Houston area [*Ryerson et al.*, 2003; *Tropp et al.*, 1998; *Allen*, 2005], and so resulted in reduced correlations between simulated and observed concentrations (Figure 5). In addition, the impact of the sea breeze might also be another factor that resulted in the lower correlation along the coastal regions. After removing two $PM_{2.5}$ stations in the western tip of Texas (107°E west), the overall R value in the remaining 34 stations in Texas is 0.77 (Figure 6a). Such a high correlation clearly demonstrates that the daily fluctuation of $PM_{2.5}$ mass are well simulated in RAMS-AROMA, particularly along the smoke pathway region (the correlation are all at >99.99% confidence level, Figure 6). It also indicates that the long-range transported CABB smoke aerosols are the major contributors affecting the air quality in Texas during the study time period.

[37] The linear relationship between daily averaged $PM_{2.5}$ mass and modeled smoke concentration varies by station, but in general the slope is about 1.5∼3 (Figures 6b–6g), except in northern and western Texas where the slope varies from 3∼4.5 (Figures 6h and 6i). The slopes indicate that on average, the contribution of smoke mass to $PM_{2.5}$ mass is much larger in southern and central Texas than that in western and northern Texas, which is consistent with the previous analysis in Figure 2. If we interpret the intercept in the linear equation as the concentration of background $PM_{2.5}$ mass, (e.g., aerosol mass concentration in no smoke condition), the model results suggested that the transported smoke resulted in an increase in $PM_{2.5}$ mass over background by about 25–35% (Figure 6a).

4.2.2. Comparison With IMPROVE Carbon and KNON

[38] Various studies have shown that high concentrations of both KNON and carbon are reliable indicators of smoke

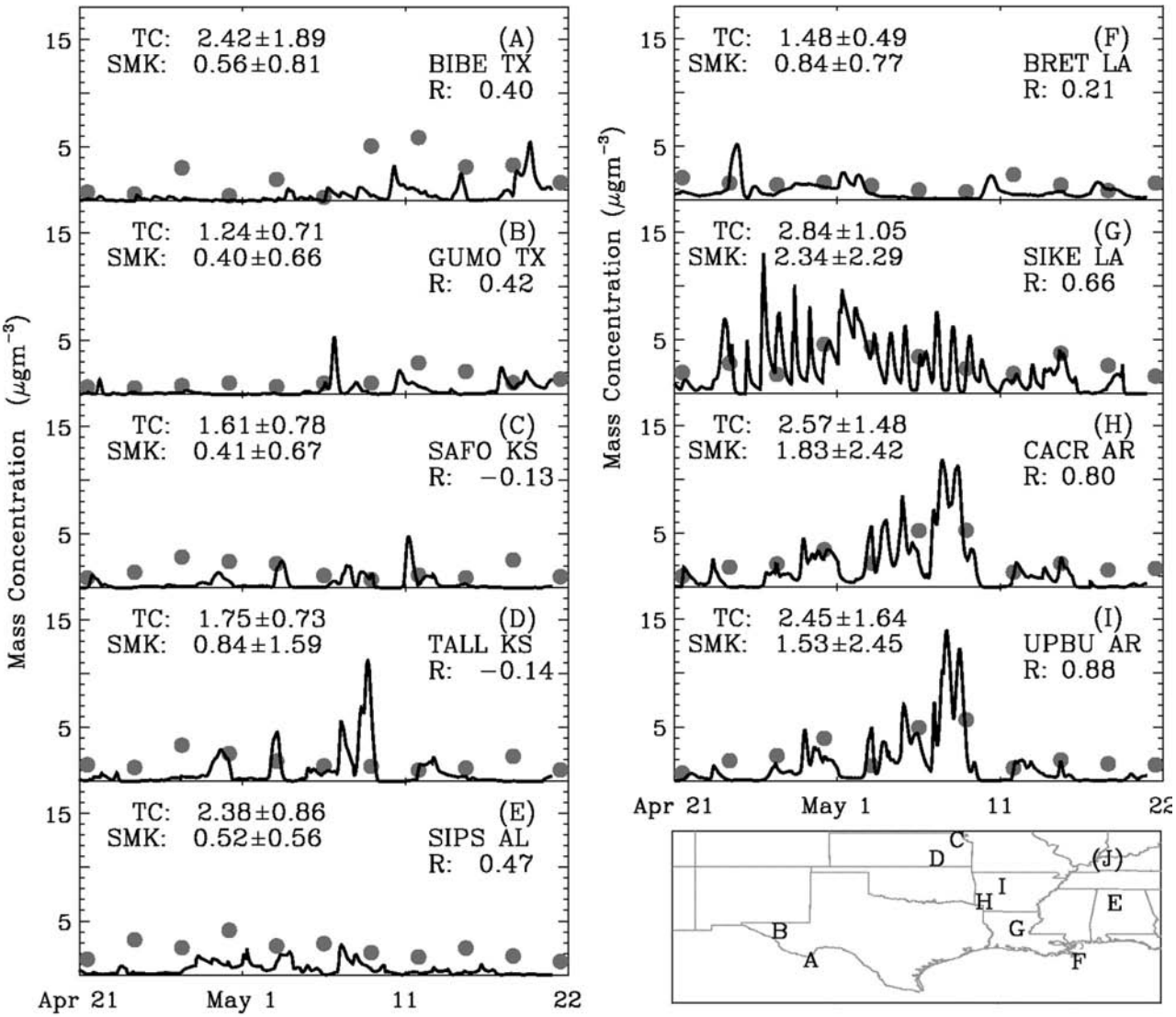

Figure 7. (a–i) Time series of modeled smoke mass concentration (SMK, continuous line) and the measured concentration of total carbon (TC, solid dots) in different IMPROVE sites. Also shown are the correlation coefficient R between these two variables as well as the mean ± standard deviation of each variable. (j) Locations of each IMPROVE stations corresponding to Figures 7a–7i.

aerosols [*Kreidenweis et al.*, 2001]. Figure 7 shows the time series of simulated smoke concentrations and measured total aerosol carbon at nine IMPROVE sites over the SEUS. Overall, the modeled smoke concentration correlates well with measured total carbon mass and KNON at three IMPROVE sites along the smoke pathway, with R values of 0.66, 0.8, and 0.88 in SIKE, CACR, and UPBU stations, respectively (Figures 7g–7i); while comparisons at other sites show no significant correlations (Figures 7a–7f) possibly because of two factors. First, the model indicates that there is less smoke transported to these stations. The averaged smoke concentration is less than 1 $\mu g\ m^{-3}$ in Figures 7a–7f, while all are larger than 2.5 $\mu g\ m^{-3}$ in Figures 7g–7i. Therefore, for those stations not along the smoke pathway, the variations of local emission may outweigh the transported smoke and dominate the fluctuations of total carbon. Second, the every-third-day sampling procedure employed by the IMPROVE network may not be sufficient enough to capture all the smoke events. For instance, there were no samplings during the smoke events on 7–8 May and 10–11 May. Consequently, in the following analysis, we will mainly focus on results for the SIKE, CACR, and UPBU stations, the stations that were frequently affected by the smoke events.

[39] The comparison shows that the overall correlations of modeled smoke concentration to the KNON and total carbon at SIKE, CACR, and UPBU sites are 0.69, and 0.74, respectively (Figures 8a and 8b). Such comparisons could be influenced by several factors such as the variation of K and the carbon percentage in smoke particles from different biomass fuels. In addition, the atmospheric carbon may originate from many sources, not only transported smoke particles, but also secondary production and local emissions such as biogenic sources (carbon from nonsmoke sources will be referred to as background carbon). As noted by *Kreidenweis et al.* [2001], the industrial pollutants in

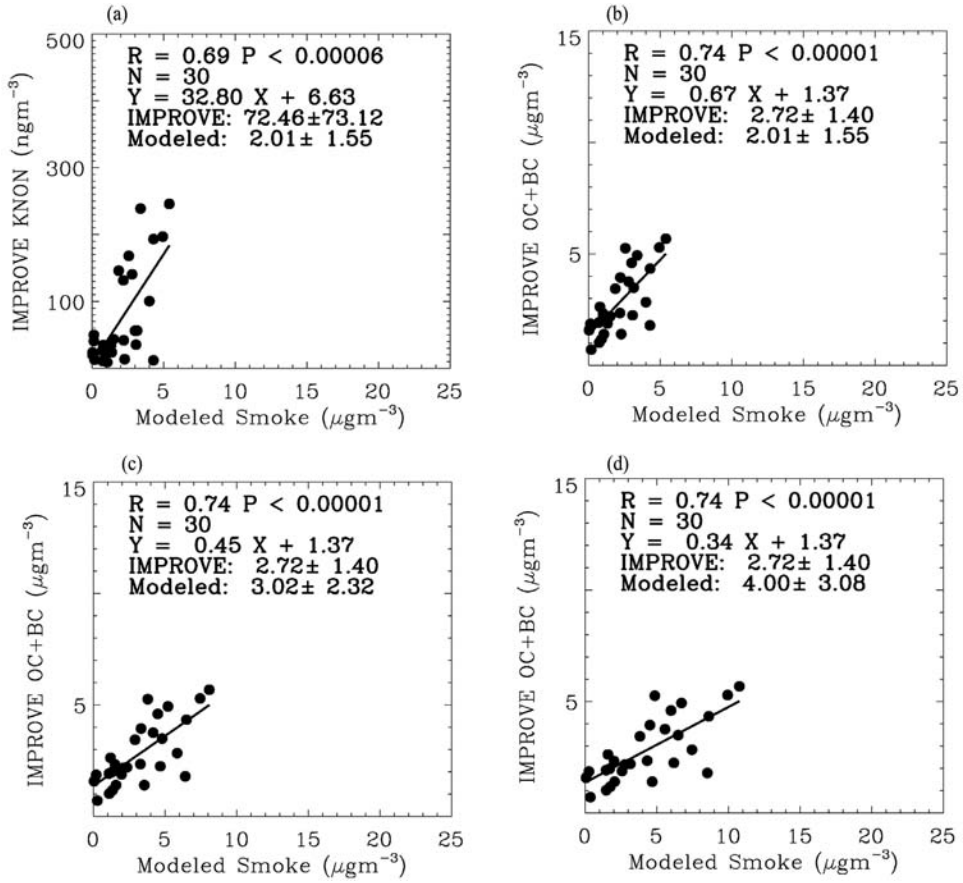

Figure 8. Comparison of modeled smoke concentration (x axis) from RAMS-AROMA baseline simulation with the measured mass concentrations of (a) KNON and (b) total carbon at three IMPROVE sites (SIKE, CACR, and UPBU). (c and d) Same as Figure 8b except that the modeled smoke concentration are from simulations with 1.5 and 2.0 of baseline smoke emissions, respectively.

Mexico, when mixed with CABB smoke aerosols, can be transported to the SEUS, and to some extent increase the level of K and carbon in the smoke plumes. Therefore a multiyear analysis of IMPROVE data is used in this study to investigate these uncertainties.

[40] The average mass concentrations of $PM_{2.5}$ sulfate particles and total carbon in April and May from 2000 to 2002 at the SIKE, CACR, and UPBU sites along the smoke pathway are shown in Figure 9 (hereinafter these 3-year averaged values are called climatological values). The impact of upwind industrial pollution sources on the concentrations at those sites is evaluated by the comparison of the sulfate concentrations observed on smoke pollution days (as judged from modeled smoke distribution and large-scale $PM_{2.5}$ observations) with the climatological values. Compared to climatological values, the $PM_{2.5}$ mass concentrations during smoke pollution days are increased at all three sites by ~30 to 80% (Figure 9). The differences in these percentages could potentially be due to the inhomogeneous spatial distribution of smoke. Figure 9 shows that the increase of $PM_{2.5}$ mass mainly results from the substantial increase of carbon (greater than ~60%) at all three sites, which is expected since the majority of smoke mass is carbon. Interestingly, the sulfate concentration also increased (at least >10%) at all three sites during the smoke events. This is consistent with the hypothesis of *Kreidenweis et al.* [2001] indicating that the comparison in Figure 8 could be affected by upwind industrial sources. In addition, *Reid et al.* [1998] also showed that sulfate is an integral part of biomass burning smoke, and its mass contribution could be 10–20% of smoke particle mass after smoke plumes pass through cloud layers. Accurate quantification of such impacts is beyond the scope of this study, since detailed emission inventories of industrial pollution in Central America are required. Nevertheless, the relatively high correlations at three sites along the smoke pathway indicate that the model reasonably simulates the timing and relative magnitude of the smoke distribution, even though detailed chemistry processes (such as secondary production of carbon) are not considered in this study.

5. Sensitivity Analysis of Smoke Emission

5.1. Top-Down Estimation of Smoke Emission Uncertainty

[41] Since the majority of smoke particle mass is composed of carbon, several studies have used the IMPROVE carbon data to calibrate the smoke emission [e.g., *Park et al.*, 2003; *Carmichael et al.*, 2003]. However, the total carbon from the IMPROVE data includes not only the carbon originated from smoke aerosols (SMK-Carbon) but also the background carbon (BG-Carbon). The knowledge

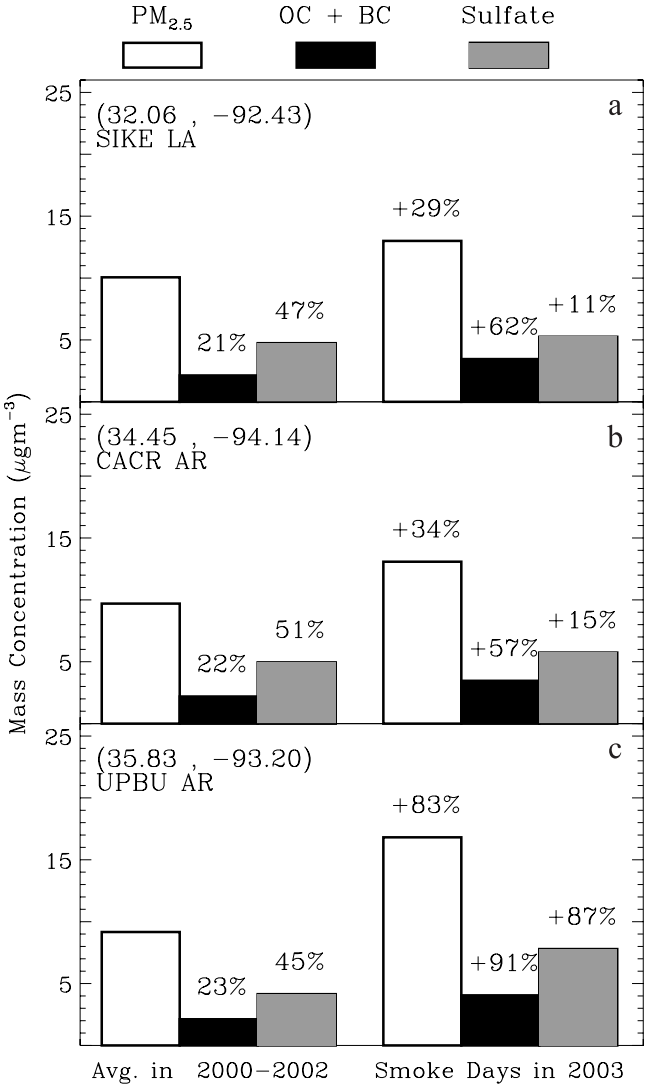

Figure 9. (a) Averaged mass concentration of $PM_{2.5}$, carbon and sulfate aerosols at IMPROVE site SIKE LA in two time periods, one in April–May of 2000–2002 and another in smoke days during 20 April to 20 May 2003. Also shown in the first time period is the mass percentage of carbon and sulfate aerosols relative to the $PM_{2.5}$ mass concentration. In the second time period, only the increased percentages (with plus sign) of $PM_{2.5}$, carbon and sulfate mass relative to their corresponding values in the first time period are shown. See text for details. (b and c) Same as Figure 9a but for the other two IMPROVE sites, CACR AR and UPBU AR, respectively. The numbers in the bracket of each panel show the latitude and longitude of each IMPROVE site.

of the BG-Carbon mass is therefore required before the IMPROVE-measured carbon can be used as a constraint for the estimation of smoke emission uncertainties. Although the multiyear averaged total carbon mass concentration (or climatological values) to some extent can be considered as the amount of BG-Carbon [e.g., *Malm et al.*, 2004], this is only applicable in the regions that do not contain long-distance transported aerosols. For regions such as SIKE, CACR and UPBU, sites that are affected by the CABB smoke aerosols in every spring season, their climatological amount of carbon should be larger than the amount of BG-Carbon. Nevertheless, the climatological values in SIKE, CACR, and UPBU sites indicate a remarkable consistency, all showing that the $PM_{2.5}$ mass is $\sim$10 $\mu g\ m^{-3}$ among which total carbon is 2.2 $\mu g\ m^{-3}$ (or 22%) and sulfate particle mass is $\sim$47% (Figure 9). This consistency allowed us to group the measured carbon at SIKE, CACR, and UPBU sites together in the top-down analysis, and to hypothesize that the BG-Carbon mass averaged at these three sites during the 30-day time period should be less than 2.2 $\mu g\ m^{-3}$.

[42] To further quantify the BG-Carbon, a best fit linear equation was computed between model-simulated smoke concentrations and IMPROVE total carbon concentrations at the three IMPROVE sites (Figure 8b). The intercept of 1.3 $\mu g\ m^{-3}$ in the best fit linear equation (Figure 8b) can be interpreted as the amount of BG-Carbon mass, since both quantities are the total carbon mass in no smoke conditions. This BG-Carbon mass is consistent with the above hypothesis that its value should be less than 2.2 $\mu g\ m^{-3}$. This estimate is also consistent with recent measurements by *Russel and Allen* [2004] who showed that the BG-Carbon in the southern Texas was in the range of 1.1–1.6 $\mu g\ m^{-3}$ (with mean value of 1.3 $\mu g\ m^{-3}$) during April–May timeframe in 2001 and 2002 [cf. *Russel and Allen*, 2004, Figure 6]. The contribution of SMK-Carbon to the climatological values of total carbon is difficult to measure directly, and the simulation from global aerosol models by *Park et al.* [2003] showed that this contribution is about 1.0 $\mu g\ m^{-3}$ along the smoke pathway [e.g., *Park et al.*, 2003]. On the basis of the analyses above, our best estimate of the BG-Carbon mass averaged in the SIKE, CACR, and UPBU during April–May is about 1.2 $\mu g\ m^{-3}$.

[43] Using the estimated GB-Carbon mass and considering that the total carbon mass averaged at the three IMPROVE sites during the 30-day study time period is approximately 2.7 $\mu g\ m^{-3}$ (Figure 8d), we estimate that the SMK-Carbon is about 1.5 $\mu g\ m^{-3}$ during the smoke events in 2003. The ratio of smoke particle mass to the SMK-carbon mass varies with different fuel types, burning characteristics as well as meteorological conditions, and the reported values usually are in the range from 1.4 to 2.0 [*Reid et al.*, 2005a]. If we use the median value of 1.7 as the ratio for this study, then the smoke mass averaged at the three IMPROVE sites should be about 2.6 $\mu g\ m^{-3}$ (in order to render 1.5 $\mu g\ m^{-3}$ SMK-Carbon). This value of smoke mass is larger than 2.0 $\mu g\ m^{-3}$ in the baseline simulation, but smaller than 3.0 $\mu g\ m^{-3}$ and 4.0 $\mu g\ m^{-3}$ in Layer8-hourly-1.5E and Layer8-hourly-2.0E simulations (Figures 8c and 8d), respectively, implying that the smoke emission is possibly underestimated by 40% in the baseline case-consistent with *Reid et al.*'s [2004] finding for the Amazon Basin. However, the above estimate varies with the ratio of smoke particle mass to SMK-Carbon mass, and if we choose a ratio of 2.3 suggested by *Turpin and Lim* [2001], then the baseline emission may underestimate the true emission by 70%.

[44] Because the above top-down emission analysis is based upon the surface measurements only, any errors in the modeled smoke vertical profile can result in uncertainties in the emission estimates. To further quantify the emission

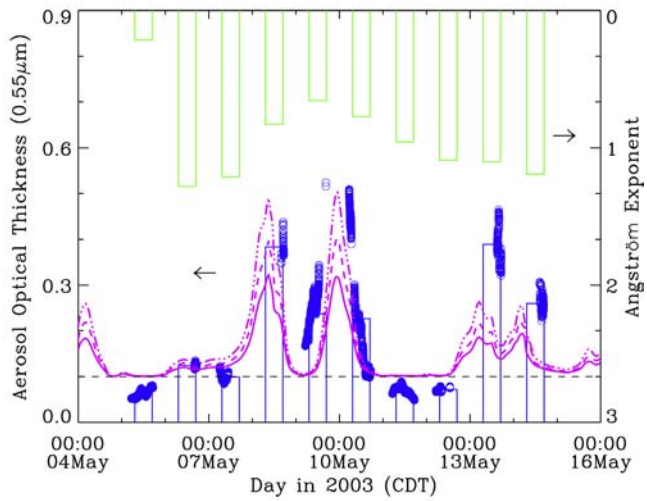

Figure 10. Measured column AOT (blue dots) and modeled smoke AOT (pink lines) at the ARM SGP site. The measured AOT at 0.55 μm is derived from the logarithmic fit between NIMFR AOT at 0.50 μm and 0.61 μm. Blue and green bars show the daily averaged AOT and Angstrom exponents derived from the ground-based AOT measurements, respectively. Since AOT values during the night were not measured, the daily averaged values (shown as bars) are only plotted across the daytime. Solid, dashed, and dot-dashed (pink) lines represent modeled AOT for baseline smoke emission, 1.5 baseline, and 2.0 baseline emission, respectively. Note that the two arrows indicate that AOT and Angstrom exponents are corresponding to different *y* axis.

uncertainties, the simulated columnar smoke AOT are compared against the measured columnar AOTs at the ARM SGP site (Figure 10). In all three experiments (e.g., baseline, Layer8-hourly-1.5E, and Layer8-hourly-2.0E), the modeled AOT consistently captured the fluctuations of measured AOT (Figure 10). In particular, if we consider the increase, maximum and decrease of AOTs as indicators of the timeline of smoke events (e.g., starting, peak, and ending time), then the model-simulated timeline of smoke events (e.g., 8–12 May 2003) is in good agreement with those identified from observed AOTs (the temporal differences are within 4–6 hours at most). Note that the Angstrom exponents decreased during the smoke events, which is consistent with the results of *Andrews et al.* [2004] who used 2 years of ARM data sets and showed that long-range transported smoke aerosols decreased the Angstrom exponent at the ARM site.

[45] Quantitatively, the long-term record of AOT data at the ARM SGP site showed that the background AOT in this region is fairly constant around 0.1 [*Andrews et al.*, 2004] (also Figure 10). In the baseline case, the model-simulated AOT is always lower than the measured AOT, even after adding the background AOT of 0.1 (as shown in Figure 10). The difference between modeled and measured AOT becomes smaller after the smoke emission was increased in both Layer8-hourly-1.5E and Layer8-hourly-2.0E experiments. In the latter case, the model almost reproduces the same time series of measured AOT on 8–10 May, which indicates that the FLAMBE emissions could underestimate the true emission by 100%. However, it should be noted that the modeled AOT values not only depend on the total smoke emission, but also can be affected by the smoke mass extinction efficiency and hygroscopicity that were formulated in the model. Therefore the modeled and measured AOT difference in Figure 10 could also be partially due to the 20–30% underestimation of smoke mass extinction efficiency used in the model (see section 3.2) as well as the additional sulfate particles associated with CABB smoke plumes that are not considered in the modeled AOT. If this is the case, an increase of baseline smoke emission by 100% would be impossible, and a 50–70% increase would be more reasonable.

[46] Given all the uncertainties mentioned in the above analyses, an exact quantification of total smoke emission seems difficult at this point. While the intercomparison between the modeled and the measured mass quantities at three IMPROVE sites indicate a 40–70% underestimation in the baseline emission, the analysis of AOT intercomparison at the ARM SGP site showed an underestimation about 50–70%. To reconcile these estimate differences, collaborative efforts involving numerical modeling and in situ measurements of smoke particle chemical, physical and optical properties are needed. An increase in the baseline smoke emission by about 60 ± 10% would provide our best estimate of smoke emissions. According to this best estimate, the total CABB smoke emission during 20 April to 21 May 2003 is about 1.3 ± 0.2 Tg, which is less than the value suggested by *Park et al.* [2003] for smoke emission during the big fire events in May 1998, but is higher than values in the normal years (on the basis of the extrapolation of data from HL94).

5.2. Impact of Diurnal Variations and Injection Height in Smoke Emission

[47] Compared to the baseline experiment, the Layer8-Daily-1.0E experiment shows a slightly higher correlation between the modeled smoke mass and measured quantities (R = 0.77 for both carbon and KNON, 0.78 for $PM_{2.5}$ in Texas, Table 2) in the downwind SEUS region. Further comparisons indicate that there are 12 stations in Texas showing R larger than 0.8 between $PM_{2.5}$ and modeled smoke concentration in Layer8-Daily-1.0E simulation, in contrast to 7 stations in the baseline simulation (Figure 11). This analysis seems to suggest that Layer8-Daily-1.0E provides a better simulation of smoke distribution in the downwind region, albeit there are measurable differences of smoke mass concentration between Layer8-Daily-1.0E and baseline experiments. (Table 2).

[48] The mean value of near-surface smoke mass concentration at 34 $PM_{2.5}$ stations in Texas (not including 2 stations in Western Texas) is 3.6 μg m^{-3} in Layer8-Daily-1.0E simulation, which is about 20% higher than 3.0 μg m^{-3} in the baseline experiment (Table 2). In contrast, the collocated smoke concentration at the three IMPROVE sites along the smoke pathway stations is 2.1 μg m^{-3} in the Layer8-Daily-1.0E experiment, only about 7% higher than 2.0 μg m^{-3} in the baseline experiment (Table 2). These statistical differences in comparisons at the IMPROVE sites and $PM_{2.5}$ sites might be due to their sample differences, i.e., IMPROVE only carries out a measurement every third day, while $PM_{2.5}$ is measured on an hourly basis. However, in either com-

Table 2. Comparison Statistics Between Measured Quantities (Y) and Modeled Smoke Concentration (X) in Different Simulation Experiments[a]

Measured Quantity	Experiments	N	R	Linear Equation	Modeled Smoke, $\mu g\ m^{-3}$
IMPROVE carbon	Layer8-Hourly-1.0E	30	0.74	Y = 0.67X + 1.37	2.01 ± 1.55
IMPROVE carbon	Layer8-Daily-1.0E	30	0.77	Y = 0.66X + 1.30	2.15 ± 1.63
IMPROVE carbon	Layer7-Hourly-1.0E	30	0.70	Y = 0.61X + 1.42	2.13 ± 1.61
IMPROVE carbon	Layer9-Hourly-1.0E	30	0.75	Y = 0.74X + 1.41	1.77 ± 1.42
IMPROVE KNON	Layer8-Hourly-1.0E	30	0.69	Y = 32.80X + 6.63	2.01 ± 1.55
IMPROVE KNON	Layer8-Daily-1.0E	30	0.77	Y = 34.39X − 1.32	2.15 ± 1.63
IMPROVE KNON	Layer7-Hourly-1.0E	30	0.63	Y = 28.61X + 11.45	2.13 ± 1.61
IMPROVE KNON	Layer9-Hourly-1.0E	30	0.72	Y = 37.10X + 6.67	1.77 ± 1.42
$PM_{2.5}$ in 34 stations in Texas	Layer8-Hourly-1.0E	1005	0.76	Y = 2.90X + 9.15	3.02 ± 2.90
$PM_{2.5}$ in 34 stations in Texas	Layer8-Daily-1.0E	1005	0.78	Y = 2.56X + 8.69	3.61 ± 3.42
$PM_{2.5}$ in 34 stations in Texas	Layer7-Hourly-1.0E	1005	0.75	Y = 2.50X + 9.40	3.40 ± 3.35
$PM_{2.5}$ in 34 stations in Texas	Layer9-Hourly-1.0E	1005	0.75	Y = 3.56X + 0.02	2.50 ± 2.35

[a]See text for details. N, number of comparison pairs; R, linear correlation coefficient. Also shown is the best fit linear equation and averaged smoke concentration in each comparison.

parison, the smoke concentrations near the surface in the Layer8-Daily-1.0E case are systemically higher than those in the baseline case, possibly because of the fact that the daily emission inventory does not capture the diurnal variations of smoke emission. In the Layer8-Daily-1.0E experiment, the total emitted smoke amount is equally distributed in both day and night. Since the biomass burning mainly occurs during the daytime, and the emission rate should be close to zero [*Prins et al.*, 1998] during the night, the "equally distributed" emission scheme artificially distributes more smoke during the night, and less smoke during the daytime. Because the turbulent mixing is much weaker during the night than during the day [*Stull*, 1989], the impact of distributing more smoke particles during the night would lead to much higher smoke concentration near the surface, and overwhelm the impact caused by the decreased smoke emission during the daytime. As the result, the simulation with a daily emission inventory provides a higher smoke concentration near the surface (even in the downwind regions) than those in the baseline experiment using an hourly smoke emission inventory.

[49] Because of the lack of hourly chemical speciation data in downwind regions, the above analyses can only be made on daily scales. This prevents us from drawing a solid conclusion on whether diurnal variation of smoke emission is important or not in the smoke simulation. As suggested by *Heald et al.* [2003], one important feature regarding the long-range aerosol transport is dynamical mixing, that tends to result in a relatively homogenous aerosol distribution in the downwind region. Therefore, under the influence of dynamical mixing, the impact of diurnal variation of smoke emission on the temporal variation of smoke distribution becomes smaller and smaller as the smoke plumes move further from the source region (e.g., Yucatan Peninsula). This might explain why the simulations using a daily smoke emission inventory indicate similar or even slightly better performance in the downwind SUES regions than the simulation using an hourly smoke inventory. In addition, because our daily emission inventory is built upon the hourly emission inventory derived from the GOES satellite, it has a better chance of characterizing the fire distribution and emission than those daily emission inventories built from polar-orbiting satellites that view the same region only once or twice per day. In our other experiments (not shown) using an emission inventory from the hourly emission inventory at a particular time (1000–1100 LT) as a proxy for those daily emission inventories based on the polar-orbiting satellite fire products, we found that the simulation results, compared to baseline experiment, were in less agreement with the observations.

[50] On the basis of the aforementioned discussion we speculate that an hourly smoke inventory should be critical for realistic simulation of the smoke distribution near the source regions where the impact of dynamical mixing is relatively small, and the diurnal variation of smoke emission has more influence on the smoke temporal variation. However, the lack of aerosol measurements in Central America makes quantitative verification of this hypothesis difficult. Instead, we qualitatively elucidate this hypothesis by examining the diurnal variation of simulated AOT in the smoke source region. Both satellite measurements and ground-based observations have shown that biomass-burning fires in the tropics have a distinct diurnal variation with a peak around local noon time [*Kauffman et al.*, 2003; *Prins et al.*, 1998]. Consequently, in the smoke source region, the smoke

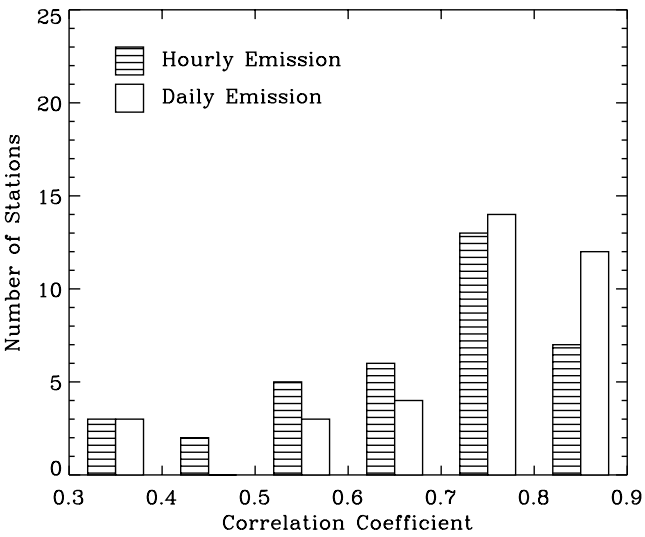

Figure 11. Frequency distribution of correlation coefficients between modeled smoke and measured $PM_{2.5}$ concentration at 36 stations in Texas for simulations with hourly and with daily emission, respectively.

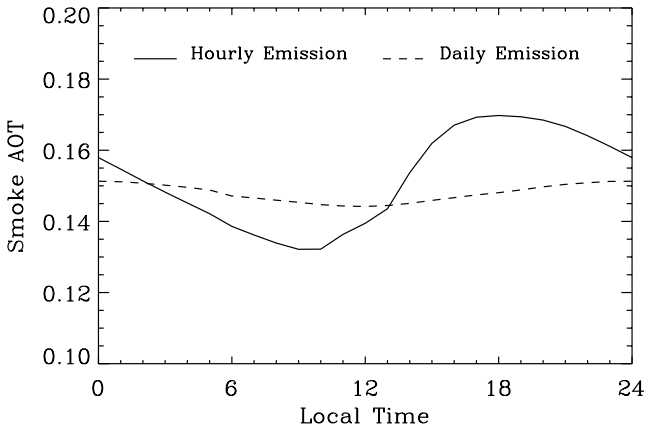

Figure 12. Diurnal variation of AOT in the smoke source region simulated in two model experiments using hourly and daily smoke emission inventories, respectively. The AOT at each hour is computed by averaging the AOTs at that hour in 30 days.

AOT symmetrically shows high values during late afternoon and evening [*Eck et al.*, 2003]. Shown in Figure 12 is the model-simulated smoke AOT in the smoke source region (Yucatan Peninsula and southern Mexico) averaged over 30 days. It indicates that the baseline simulation shows minimum AOT values of 0.13 at 1000 LT and a maximum value of 0.17 at 1800 LT, with a mean AOT of 0.15 and a diurnal variation of 0.04 (or ~25%). Such diurnal variation patterns and magnitude are comparable to the observations by *Eck et al.* [2003] during southern African biomass burning seasons. In contrast, the Layer8-Daily-1.0E experiment using a daily smoke emission inventory fails to simulate the diurnal variation of smoke AOT (Figure 12), indicating that it is critical to use high temporal resolution emission database for assessing air quality.

[51] Two experiments, Layer7-Hourly-1.0E and Layer9-Hourly-1.0E, are conducted to investigate the impact of the injection height of smoke emission on the RAMS-AROMA performance. Qualitatively, these two experiments show similar results to the baseline Layer8-hourly-1.0E experiment. Quantitative comparisons with observations are shown in Table 2. Compared to the baseline experiment, the model-simulated smoke concentration showed slightly lower correlation to $PM_{2.5}$ mass concentration in Texas, IMPROVE measured carbon and KNON (R = 0.75, 0.70, and 0.63, respectively) in Layer7-Hourly-1.0E experiment, but equivalent or slightly higher correlation in the Layer9-Hourly-1.0E experiment (R = 0.75, 0.72, 0.72, respectively). The difference in smoke concentrations near the surface between the Layer7-Hourly-1.0E (Layer9-Hourly-1.0E) and the baseline experiment is within 15% (−15%). Such differences are smaller than the uncertainties in the smoke emission inventories, and therefore their impact on our top-down analysis is insignificant.

6. Discussion

[52] We have estimated the uncertainties in the FLAMBE smoke emission database by comparing the model-simulated smoke concentrations with the total carbon in areas thousands of kilometers downwind of CABB smoke emission sources. Even though the top-down approach utilized in the present study has been explored by a variety of prior research efforts [e.g., *Park et al.*, 2003], there are several aspects that require further investigation, including the parameterization of smoke emissions from subgrid-scale fires and accounting for the smoke aging effects.

[53] A common and traditional approach to ingest the smoke emission into aerosol transport models is to compute the smoke emission rate during a time interval by assuming that smoke plumes in that time interval are distributed throughout the atmospheric column over the grid point to the injection height, with well mixed or some type of predefined (such as exponential) vertical profile. This type of scheme is not expected to capture fine-scale features such as subgrid smoke plumes. At any particular time step, large model uncertainties could exist in the smoke source region where smoke plumes from different fires are possibly in different aging states and most likely are not mixed in a similar way as being assumed in the model. Therefore the current scheme for the smoke assimilation can only capture the average smoke spatial and temporal distribution in the source region. However, because of the dynamical mixing during the long-range transport, the smoke distribution in the downwind region can be considered to be dominated by the quasi-equilibrated regional haze layers. It is thus expected that the traditional "injection height" approach, although having large uncertainties in specifying the instantaneous emission rate in the smoke source region, can give a reliable simulation of smoke distribution in the downwind regions, which is also indicated by the validation analysis in this study. Consequently, the top-down approach would be more physically meaningful if we apply it to estimates of smoke emissions on regional scales and interpret the emission estimation from a statistical standpoint. In this regard, this study only gives the total smoke emission estimate for a 30-day period.

[54] We have neglected the smoke aging processes, secondary organic aerosol formation, and biogenic emissions of organic aerosols in the model. This simplification in the model can lead to various uncertainties in the conclusions we draw from the comparison between modeled and measured quantities. We have accounted for the uncertainties arising from these neglected processes through the analyses of IMPROVE data and cross validation using different data sets (section 5.1). Further quantification of these uncertainties requires better measurements of total carbon and secondary organic carbon as well as the improvement in modeling of secondary organic aerosols. Detailed chemical speciation data in daily or even hourly scales together with a better understanding of CABB smoke microphysics (such as mass extinction efficiency and the mass budget of chemical species in smoke particles) would also benefit the top-down approach used in this study.

7. Summary

[55] Using the RAMS-AROMA we have explored the application of an hourly smoke emission inventory for the numerical simulation of CABB smoke transport in 2003. Comparisons with ground-based measurements suggest that RAMS-AROMA is able to realistically simulate the smoke spatial distribution as well as the timing and the location of

smoke fronts on daily to hourly scales. Results also indicated that the model-simulated smoke concentration captures the fluctuations of daily averaged $PM_{2.5}$ in the Texas region (with averaged R larger than 0.76), implying that the forecasts made using the RAMS-AROMA model could potentially be a useful tool in assessing the air quality in the SEUS during CABB fire seasons. Uncertainties in the smoke emission are analyzed by comparing the model-simulated smoke concentration to the measured mass of carbon aerosols. The top-down analysis indicates that the baseline FLAMBE emission inventory underestimates the smoke emission by 60 ± 10%, and the best estimate of total emitted smoke is 1.3 ± 0.2 Tg. This underestimate is similar in magnitude to that found in the Amazon Basin [*Reid et al.*, 2004]. Sensitivity studies reveal that the simulation using a daily smoke emission inventory provides a slightly better correlation with measurements in the downwind region on daily scales, but gives an unrealistic diurnal variation of AOT in the smoke source region. These results suggest that the assimilation of hourly emission inventories from geostationary satellites has the unique capability for the high spatiotemporal simulation of long-range smoke transport that is not possible by using emission inventories derived from polar-orbiting satellites. However, the detailed chemical speciation data with high temporal resolutions (e.g., daily or hourly), a better understanding of smoke chemical and physical properties, as well as the modeling of smoke aging process are needed to further narrow down the model uncertainties.

[56] **Acknowledgments.** This research was supported by NASA's Radiation Sciences, Interdisciplinary sciences and ACMAP programs. J. Wang was supported by the NASA Earth System Science Graduate Fellowship and the NOAA Climate and Global Change Postdoctoral Fellowship under the administration of UCAR. The GOES WF-ABBA fire monitoring effort is supported by NOAA contract 40AANE1A4073 and by NASA's ESE Interdisciplinary Science Program through Navy subcontract N66001-00-C-0039. NRL participation was also supported by ONR 322 contract N0001405WR20206. The views, opinions, and findings contained in this report are those of the author(s) and should not be construed as an official U.S. Government position, policy, or decision. The lidar and AOT data were obtained from the DOE ARM program, and we are grateful to Rich Ferrare, David Turner, Joseph Michalsky, and James Barnard for their guidance in using the data.

References

Ackerman, A. S., O. B. Toon, D. E. Stevens, A. J. Heymsfield, V. Ramanathan, and E. J. Welton (2000), Reduction of tropical cloudiness by soot, *Science*, *288*, 1042–1047.

Ahern, F. J., J. G. Goldammer, and C. O. Justice (Eds.) (2001), *Global and Regional Vegetation Fire Monitoring From Space: Planning an Coordinated International Effort*, SPB Acad., The Hague, Netherlands.

Allen, D. (2005), Gulf coast aerosol research and characterization program (Houston supersite), final report, *Coop. Agreement 82806201*, Environ. Prot. Agency, Washington, D. C. (Available at http://eosweb.larc.nasa.gov/PRODOCS/narsto/table_narsto.html#houston)

Allen, G. A., C. Sioutas, P. Koutrakis, R. Reiss, F. W. Lumann, and P. T. Roberts (1997), Evaluation of the TEOM method for measurement of ambient particulate mass in urban areas, *J. Air Waste Manage. Assoc.*, *47*, 682–689.

Andrews, E., P. J. Sheridan, J. A. Ogren, and R. Ferrare (2004), In situ aerosol profiles over the Southern Great Plains cloud and radiation test bed site: 1. Aerosol optical properties, *J. Geophys. Res.*, *109*, D06208, doi:10.1029/2003JD004025.

Byun, D. W., and J. K. S. Ching (1999), Science algorithms of the EPA Model-3 Community Multiscale Air Quality (CMAQ) modeling system, *Rep. EPA-600/R-99/030*, U. S. Eviron. Prot. Agency, Washington, D. C.

Carmichael, G. R., et al. (2003), Evaluating regional emission estimates using the TRACE-P observations, *J. Geophys. Res.*, *108*(D21), 8810, doi:10.1029/2002JD003116.

Charron, A., R. M. Harrison, S. Moorcroft, and J. Booker (2004), Quantitative interpretation of divergence between PM10 and PM2.5 mass measurement by TEOM and gravimetric (Partisol) instruments, *Atmos. Environ.*, *38*, 415–423.

Chin, M., P. Ginoux, S. Kinne, O. Torres, B. N. Holben, B. N. Duncan, R. V. Martin, J. A. Logan, A. Higurashi, and T. Nakajima (2002), Troposphere aerosol optical thickness from the GOCART model and comparisons with satellite and sun photometer measurements, *J. Atmos. Sci.*, *59*, 461–483.

Chow, J. C., J. G. Watson, L. C. Prichett, W. R. Pierson, C. A. Frazier, and R. G. Purcell (1993), The DRI thermal/optical reflectance carbon analysis system: Description, evaluation, and applications in U.S. air quality studies, *Atmos. Environ.*, *27*, 1185–1201.

Christopher, S. A., and J. Zhang (2002), Daytime variation of shortwave direct radiative forcing of biomass burning aerosols from GOES 8 imager, *J. Atmos. Sci.*, *59*, 681–691.

Colarco, P. R., M. R. Schoebert, B. G. Doddridge, L. T. Marufu, O. Torres, and E. J. Welton (2004), Transport of smoke from Canadian forest fires to the surface near Washington, D.C.: Injection height, entrainment, and optical properties, *J. Geophys. Res.*, *109*, D06203, doi:10.1029/2003JD004248.

Crutzen, P. J., L. E. Heidt, J. P. Krasnec, W. H. Pollock, and W. Seiler (1979), Biomass burning as a source of atmospheric gases CO, H_2, N_2O, NO, CH_3Cl and COS, *Nature*, *282*, 253–256.

Crutzen, P. J., and M. O. Andreae (1990), Biomass burning in the tropics: Impact on atmospheric chemistry and biogeochemical cycles, *Science*, *250*, 1669–1678.

Davison, P. S., D. L. Roberts, R. T. Arnold, and R. N. Colvile (2004), Estimating the direct radiative forcing due to haze from the 1997 forest fires in Indonesia, *J. Geophys. Res.*, *109*, D10207, doi:10.1029/2003JD004264.

Eck, T. F., et al. (2003), Variability of biomass burning aerosol optical characteristics in southern Africa during the SAFARI 2000 dry season campaign and a comparison of single scattering albedo estimates from radiometric measurements, *J. Geophys. Res.*, *108*(D13), 8477, doi:10.1029/2002JD002321.

Ferek, R. J., J. S. Reid, P. V. Hobbs, D. R. Blake, and C. Liousse (1998), Emission factors of hydrocarbons, halocarbons, trace gases and particles from biomass burning in Brazil, *J. Geophys. Res.*, *103*, 32,107–32,118.

Ferrare, R., D. D. Turner, L. A. Heilman, W. Feltz, O. Dubovik, and T. Tooman (2001), Raman lidar measurements of the aerosol extinction-to-backscatter ratio over the southern great plains, *J. Geophys. Res.*, *106*, 20,333–20,347.

Ferrare, R., et al. (2006), Raman Lidar measurements of aerosols and water vapor over the Southern Great Plains during the May 2003 Aerosol IOP, *J. Geophys. Res.*, *111*, D05S08, doi:10.1029/2005JD005836.

Food and Agricultural Organization (1997), State of the world's forest 1997, report, Food and Agric. Organ. of the U. N., Rome, Italy.

Forster, C., et al. (2001), Transport of boreal fire emissions from Canada to Europe, *J. Geophys. Res.*, *106*, 22,887–22,906.

Fu, Q., and K. N. Liou (1993), Parameterization of the radiative properties of cirrus clouds, *J. Atmos. Sci.*, *50*, 2008–2025.

Gao, S., D. A. Hegg, P. V. Hobbs, T. W. Kirchstetter, B. I. Magi, and M. Sadilek (2003), Water-soluble organic components in aerosols associated with savanna fires in southern Africa: Identification, evolution, and distribution, *J. Geophys. Res.*, *108*(D13), 8491, doi:10.1029/2002JD002324.

Grell, G. A., J. Dudhia, and D. Stauffer (1995), A description of the fifth-generation Penn State/NCAR Mesoscale Model (MM5), *NCAR/TN-398+STR*, 122 pp., Natl. Cent. for Atmos. Res., Boulder, Colo. (Available at http://www.mmm.ucar.edu/mm5)

Hao, W. M., and M.-H. Liu (1994), Spatial and temporal distribution of tropical biomass burning, *Global Biogeochem. Cycles*, *8*, 495–503.

Harrington, J. Y., and P. Q. Olsson (2001), A method for the parameterization of cloud optical properties in bulk and bin microphysical models. Implications for arctic cloudy boundary layers, *Atmos. Res.*, *57*, 51–80.

Heald, C. L., D. J. Jacob, P. I. Palmer, M. J. Evans, G. W. Sachse, H. B. Singh, and D. R. Blake (2003), Biomass burning emission inventory with daily resolution: Application to aircraft observations of Asian outflow, *J. Geophys. Res.*, *108*(D21), 8811, doi:10.1029/2002JD003082.

Hitzenberger, R., et al. (2004), Intercomparison of methods to measure the mass concentration of the atmospheric aerosol during INTERCOMP2000—Influence of instrumentation and size cuts, *Atmos. Environ.*, *38*, 6467–6476.

Hobbs, P. V., P. Sinha, R. J. Yokelson, T. J. Christian, D. R. Blake, S. Gao, T. W. Kirchstetter, T. Novakov, and P. Pilewskie (2003), Evolution of gases and particles from a savanna fire in South Africa, *J. Geophys. Res.*, *108*(D13), 8485, doi:10.1029/2002JD002352.

Intergovernmental Panel on Climate Change (2001), *Climate Change 2001: The Scientific Basis—Contribution of Working Group I to the Third*

Assessment Report of the Intergovernmental Panel on Climate Change, edited by J. T. Houghton et al., 881 pp., Cambridge Univ. Press, New York.

Ito, A., and J. E. Penner (2004), Global estimates of biomass burning emissions based on satellite imagery for the year 2000, *J. Geophys. Res.*, *109*, D14S05, doi:10.1029/2003JD004423.

Iziomon, M. G., and U. Lohmann (2003), Optical and meteorological properties of smoke-dominated haze at the ARM Southern Great Plains central facility, *Geophys. Res. Lett.*, *30*(3), 1123, doi:10.1029/2002GL016606.

Jacobson, M. Z. (1997), Development and application of a new air pollution modeling system part II: Aerosol module structure and design, *Atmos. Environ., Part A*, *31*, 131–144.

Jacobson, M. Z. (2001), Strong radiative heating due to the mixing state of black carbon in atmospheric aerosols, *Nature*, *409*, 695–697.

Kalnay, E., et al. (1996), The NCEP/NCAR 40-year reanalysis project, *Bull. Am. Meteorol. Soc.*, *77*, 437–471.

Kanakidou, M., et al. (2005), Organic aerosol and global climate modeling: A review, *Atmos. Chem. Phys.*, *5*, 1053–1123.

Kaufman, Y. J., D. Tanre, and O. Boucher (2002), A satellite view of aerosols in climate systems, *Nature*, *419*, 215–223.

Kauffman, J. B., M. D. Steele, D. L. Cummings, and V. J. Jaramillo (2003), Biomass dynamics associated with deforestation, fire, and conversion to cattle pasture in a Mexican tropical dry forest, *For. Ecol. Manage.*, *176*, 1–12.

Koren, I., Y. J. Kaufman, L. A. Remer, and J. V. Martins (2004), Measurement of the effect of Amazon smoke on inhabitation of cloud formation, science, *Science*, *303*, 1342–1345.

Kotchenruther, R. A., and P. V. Hobbs (1998), Humidification factors of aerosols from biomass burning in Brazil, *J. Geophys. Res.*, *103*, 32,081–32,089.

Kreidenweis, S. M., L. A. Remer, R. Bruintjes, and O. Dubovik (2001), Smoke aerosols from biomass burning in Mexico: Hygroscopic smoke optical model, *J. Geophys. Res.*, *106*, 4831–4844.

Lavoue, D., C. Liousse, H. Cachier, B. J. Stocks, and J. G. Goldammer (2000), Modeling of carbonaceous particles emitted by boreal and temperate wildfires at northern latitudes, *J. Geophys. Res.*, *105*, 26,871–26,890.

Levinson, D. H., and A. M. Waple (Eds.) (2004), State of the climate in 2003, *Bull. Am. Meteorol. Soc.*, *85*, S1–S72.

Liousse, C., J. E. Penner, C. C. Chuang, J. J. Walton, and H. Eddleman (1996), A global three dimensional model study of carbonaceous aerosols, *J. Geophsy. Res.*, *101*, 19,441–19,432.

Malm, W. C., J. F. Sisler, D. Huffman, R. A. Eldred, and T. A. Cahill (1994), Spatial and seasonal trends in particle concentration and optical extinction in the United States, *J. Geophys. Res.*, *99*, 1357–1370.

Malm, W. C., B. A. Schichtel, M. L. Pitchford, L. L. Ashbaugh, and R. A. Eldred (2004), Spatial and monthly trends in speciated fine particle concentration in the United States, *J. Geophys. Res.*, *109*, D03306, doi:10.1029/2003JD003739.

Mellor, G. L., and T. Yamada (1974), A hierarchy of turbulent closure models for planetary boundary layers, *J. Atmos. Sci.*, *31*, 1791–1806.

Myhre, G., T. K. Berntsen, J. M. Haywood, J. K. Sundet, B. N. Holben, M. Johnsrud, and F. Stordal (2003), Modeling the solar radiative impact of aerosols from biomass burning during the Southern African Regional Science Initiative (SAFARI-2000) experiment, *J. Geophys. Res.*, *108*(D13), 8501, doi:10.1029/2002JD002313.

Park, R. J., D. J. Jacob, M. Chin, and R. V. Martin (2003), Sources of carbonaceous aerosols over the United States and implications for natural visibility, *J. Geophys. Res.*, *108*(D12), 4355, doi:10.1029/2002JD003190.

Penner, J. E., R. Dickinson, and C. O'Neill (1992), Effects of aerosol from biomass burning on the global radiation budget, *Science*, *256*, 1423–1434.

Peppler, R. A., et al. (2000), ARM Southern Great Plains site observations of the smoke pall associated with the 1998 Central American fires, *Bull. Am. Meteorol. Soc.*, *81*, 2563–2592.

Pielke, R. A., R. L. Walko, J. L. Eastman, W. A. Lyons, R. A. Stocker, M. Uliasz, and C. J. Tremback (1992), A comprehensive meteorological modeling system—RAMS, *Meteorol. Atmos. Phys.*, *49*, 69–91.

Prins, E. M., J. M. Feltz, W. P. Menzel, and D. E. Ward (1998), An overview of GOES-8 diurnal fire and smoke results for SCAR-B and the 1995 fire season in South America, *J. Geophys. Res.*, *103*, 31,821–31,835.

Pruppacher, H. R., and J. D. Klett (1978), *Microphysics of Clouds and Precipitation*, 714 pp., Springer, New York.

Pun, B. K., S.-Y. Wu, C. Seigneur, J. H. Seinfeld, R. J. Griffin, and S. N. Pandis (2003), Uncertainties in modeling secondary organic aerosols: Three-dimensional modeling studies in Nashville, TN, *Environ. Sci. Technol.*, *37*, 3647–3661.

Reid, J. S., and P. V. Hobbs (1998), Physical and optical properties of young smoke from individual biomass fires in Brazil, *J. Geophys. Res.*, *103*, 32,013–32,030.

Reid, J. S., P. V. Hobbs, R. J. Ferek, D. R. Blake, J. V. Martins, M. R. Dunlap, and C. Liousse (1998), Physical, chemical, and optical properties of regional hazes dominated by smoke in Brazil, *J. Geophys. Res.*, *103*, 32,059–32,080.

Reid, J. S., T. F. Eck, S. A. Christopher, P. V. Hobbs, and B. R. Holben (1999), Use of the Angstrom exponent to estimate the variability of optical and physical properties of aging smoke particles in Brazil, *J. Geophys. Res.*, *104*, 27,473–27,490.

Reid, J. S., E. M. Prins, D. L. Westphal, C. C. Schmidt, K. A. Richardson, S. A. Christopher, T. F. Eck, E. A. Reid, C. A. Curtis, and J. P. Hoffman (2004), Real-time monitoring of South American smoke particle emissions and transport using a coupled remote sensing/box-model approach, *Geophys. Res. Lett.*, *31*, L06107, doi:10.1029/2003GL018845.

Reid, J. S., R. Koppmann, T. F. Eck, and D. P. Eleuterio (2005a), A review of biomass burning emissions part II: Intensive physical properties of biomass burning particles, *Atmos. Chem. Phys.*, *5*, 799–825.

Reid, J. S., T. F. Eck, S. A. Christopher, R. Koppmann, O. Dubovik, D. P. Eleuterio, B. N. Holben, E. A. Reid, and J. Zhang (2005b), A review of biomass burning emissions part III: Intensive optical properties of biomass burning particles, *Atmos. Chem. Phys.*, *5*, 827–849.

Robock, A. (1988), Enhancement of surface cooling due to forest fire smoke, *Science*, *242*, 911–913.

Rogers, C. M., and K. P. Bowman (2001), Transport of smoke from the Central American fires of 1998, *J. Geophys. Res.*, *106*, 28,357–28,368.

Russel, M., and D. T. Allen (2004), Seasonal and spatial trends in primary and secondary organic carbon concentrations in southeast Texas, *Atmos. Environ.*, *38*, 3225–3239.

Ryerson, T. B., et al. (2003), Effect of petrochemical industrial emissions of reactive alkenes and NO_x on tropospheric ozone formation in Houston, Texas, *J. Geophys. Res.*, *108*(D8), 4249, doi:10.1029/2002JD003070.

Schell, B., I. J. Ackermann, H. Hass, F. S. Binkowski, and A. Ebel (2001), Modeling the formation of secondary organic aerosol within a comprehensive air quality model, *J. Geophys. Res.*, *106*, 28,275–28,293.

Schmid, B., et al. (2006), How well do state-of-the-art techniques measuring the vertical profile of tropospheric aerosol extinction compare?, *J. Geophys. Res.*, *111*, D05S07, doi:10.1029/2005JD005837.

Schmid, H., et al. (2001), Results of the "carbon conference" international aerosol carbon round robin test stage I, *Atmos. Environ.*, *35*, 2111–2121.

Slinn, S. A., and W. G. N. Slinn (1980), Predictions for particle deposition on natural waters, *Atmos. Environ.*, *14*, 1013–1016.

Slinn, W. G. N. (1984), Precipitation scavenging, in *Atmospheric Science and Power Production*, edited by D. Danderson, pp. 466–532, Tech. Inf. Cent. Off. of Sci. and Tech. Inf., Dep. of Energy, Washington, D. C.

Strader, R., F. Lurmann, and S. N. Pandis (1999), Evaluation of secondary organic aerosol formation in winter, *Atmos. Environ.*, *33*, 4849–4863.

Stull, R. B. (1989), *An Introduction to Boundary Layer Meteorology*, 666 pp., Springer, New York.

Tanner, R. L., W. J. Parkhurst, M. L. Valente, K. L. Humes, K. Jones, and J. Gilbert (2001), Impact of the 1998 Central American fires on PM2.5 mass and composition in the southeastern United States, *Atmos. Environ.*, *35*, 6539–6547.

Tegen, I., P. Hollrig, M. Chin, I. Fung, D. Jacob, and J. Penner (1997), Contribution of different aerosols to the global aerosol extinction optical thickness: Estimates from model results, *J. Geophys. Res.*, *102*, 23,895–23,915.

Trentmann, J., M. O. Andreae, H.-F. Graf, P. V. Hobbs, R. D. Ottmar, and T. Trautmann (2002), Simulation of a biomass-burning plume: Comparison of model results with observations, *J. Geophys. Res.*, *107*(D2), 4013, doi:10.1029/2001JD000410.

Tropp, R. J., S. D. Kohl, J. C. Chow, and C. A. Frazier (1998), Final report for the Texas PM2.5 sampling and analysis study, *Doc. 6570-685-7770.1F*, Bur. of Air Qual. Control, Houston, Tex. (Available at http://eosweb.larc.nasa.gov/GUIDE/dataset_documents/narsto_texas_guide.html)

Turco, R. P., and F. Yu (1999), Particle size in an expanding plume undergoing simultaneous coagulation and condensation, *J. Geophys. Res.*, *104*, 19,227–19,241.

Turpin, B. J., and H.-J. Lim (2001), Species contributions to $PM_{2.5}$ mass concentration: Revisiting common assumptions for estimating organic mass, *Aerosol Sci. Technol.*, *35*, 602–610.

Turpin, B. J., P. Saxena, and E. Andrews (2000), Measuring and simulating particulate organics in the atmosphere: Problems and prospects, *Atmos. Environ.*, *34*, 2983–3013.

Twomey, S. (1977), The influence of pollution on the shortwave albedo of clouds, *J. Atmos. Sci.*, *34*, 1149–1152.

Uno, I., et al. (2003), Regional chemical weather forecasting system CFORS: Model description and analysis of surface observations at Japanese island stations during the ACE-Asia experiment, *J. Geophys. Res.*, *108*(D23), 8668, doi:10.1029/2002JD002845.

Walko, R. L., W. R. Cotton, M. P. Meyers, and J. Y. Harrington (1995), New RAMS cloud microphysics parameterization, part I: The single-moment scheme, *Atmos. Res.*, *38*, 29–62.

Walko, R. L., et al. (2000), Coupled atmosphere-biophysics-hydrology models for environmental modeling, *J. Appl. Meteorol.*, *39*, 931–944.

Wang, J., U. Nair, and S. A. Christopher (2004), GOES 8 Aerosol optical thickness assimilation in a mesoscale model: Online integration of aerosol radiative effects, *J. Geophys. Res.*, *109*, D23203, doi:10.1029/2004JD004827.

Watson, J. G., J. C. Chow, H. Moosmuller, M. Green, N. Frank, and M. Pitchfort (1998), Guidance for using continuous mintors in PM2.5 monitoring networks, *EPA-454/R-98-012*, Off. of Air Qual. Plann. and Stand., U. S. Environ. Prot. Agency, Washington, D. C.

Westphal, D. L., and O. B. Toon (1991), Simulation of microphysical, radiative, and dynamical processes in a continental-scale forest smoke plume, *J. Geophys. Res.*, *96*, 22,379–22,400.

Yu, S., R. L. Dennis, P. V. Bhave, and B. K. Eder (2004), Primary and secondary organic aerosols over the United States: Estimates on the basis of observed organic carbon (OC) and elemental carbon (BC), and air quality modeled primary OC/EC ratios, *Atmos. Environ.*, *38*, 5257–5268.

Zhang, L., S. Gong, J. Padro, and L. Barrie (2001), A size-segregated particle dry deposition scheme for an atmospheric aerosol module, *Atmos. Environ.*, *35*, 549–560.

Zhang, Y., B. Pun, K. Vijayaraghavan, S.-Y. Wu, C. Seigneur, S. N. Pandis, M. Z. Jacobson, A. Nenes, and J. H. Seinfeld (2004), Development and application of the model of aerosol dynamics, reaction, ionization, and dissolution, *J. Geophys. Res.*, *109*, D01202, doi:10.1029/2003JD003501.

S. A. Christopher and U. S. Nair, Department of Atmospheric Science, University of Alabama, 320 Sparkman Drive, Huntsville, AL 35805, USA.

J. L. Hand, Cooperative Institute for Research in the Atmosphere (CIRA), Colorado State University, Fort Collins, CO 80523, USA.

E. M. Prins, 17207 Alexandra Way, Grass Valley, CA 95949, USA.

J. S. Reid, Aerosol and Radiation Modeling Section, Marine Meteorology Division, Naval Research Laboratory, 7 Grace Hopper Avenue, Monterey, CA 93943, USA.

J. Szykman, NASA Langley Research Center, MS-401A, Hampton, VA 23681, USA.

J. Wang, Division of Engineering and Applied Science, Harvard University, Pierce Hall, Room G3F, 29 Oxford Street, Cambridge, MA 02138, USA. (junwang@fas.harvard.edu)